Molecular Pharmacology Fast Forward. Published on April 12, 2019 as DOI: 10.1124/mol.118.115196
This article has not been copyedited and formatted. The final version may differ from this version.

MOL # 115196

Functional CRISPR and shRNA screens identify involvement of mitochondrial electron transport in the activation of evofosfamide

Francis W. Hunter, Jules B. L. Devaux, Fanying Meng, Cho Rong Hong, Aziza Khan, Peter Tsai, Troy W. Ketela, Indumati Sharma, Purvi M. Kakadia, Stefano Marastoni, Zvi Shalev, Anthony J. R. Hickey, Cristin G. Print, Stefan K. Bohlander, Charles P. Hart, Bradly G. Wouters and William R. Wilson

Auckland Cancer Society Research Centre, School of Medical Sciences, Faculty of Medical and Health Sciences, University of Auckland, Private Bag 92019, Auckland, New Zealand (F.W.H., C.R.H., A.K., I.S., W.R.W.); Maurice Wilkins Centre for Molecular Biodiscovery, University of Auckland, Private Bag 92019, Auckland, New Zealand (F.W.H., A.J.R.H., C.G.P., W.R.W.); School of Biological Sciences, Faculty of Science, University of Auckland, Private Bag 92019, Auckland, New Zealand (J.B.L.D., A.J.R.H.); Threshold Pharmaceuticals, South San Francisco, CA 94080, USA (F.M., C.P.H.); Department of Molecular Medicine and Pathology, School of Medical Sciences, Faculty of Medical and Health Sciences, University of Auckland, Private Bag 92019, Auckland, New Zealand (P.T., P.M.K., C.G.P., S.K.B.); Princess Margaret Genomics Centre, University Health Network, Toronto, ON M5G 1L7, Canada (T.W.K.); Princess Margaret Cancer Centre, University Health Network, Toronto, ON M5G 1L7, Canada (S.M., Z.S., B.G.W.); Department of Radiation Oncology, University of Toronto, Toronto, ON M5S 1A1, Canada (B.G.W.); Department of Medical Biophysics, University of Toronto, Toronto, ON M5S 1A1, Canada (B.G.W.).

Primary Laboratory of Origin: Auckland Cancer Society Research Centre, University of Auckland, Private Bag 92019, Auckland, New Zealand.

Molecular Pharmacology Fast Forward. Published on April 12, 2019 as DOI: 10.1124/mol.118.115196
This article has not been copyedited and formatted. The final version may differ from this version.

MOL # 115196

Running Title: Mitochondrial involvement in evofosfamide activation

Corresponding Author: Dr Francis W. Hunter, Auckland Cancer Society Research Centre, 85 Park Road, Grafton, Auckland 1023, New Zealand. Phone: 64.9.923.6710; E-mail: f.hunter@auckland.ac.nz

Number of Text Pages: 20

Number of Tables: 3

Number of Figures: 7

Number of References: 60

Number of Words in Abstract: 245

Number of Words in Introduction: 608

Number of Words in Discussion: 1533

Abbreviations: Br-IPM, bromo-*iso*-phosphoramide mustard; Cl-IPM, chloro-*iso*-phosphoramide mustard; cyt *a*, cytochrome *a*; cyt *b*, cytochrome *b*; cyt *c*, cytochrome *c*; DMF, dose-modifying factor; FAD, flavin adenine dinucleotide; FMN, flavin mononucleotide; GO, gene ontology; PC1, first principal component; POR, P450 oxidoreductase; RNAseq, RNA sequencing; SF, surviving fraction; sgRNA, single guide RNA.

Molecular Pharmacology Fast Forward. Published on April 12, 2019 as DOI: 10.1124/mol.118.115196
This article has not been copyedited and formatted. The final version may differ from this version.

Abstract

Evofosfamide (TH-302) is a hypoxia-activated DNA-crosslinking prodrug currently in clinical development for cancer therapy. Oxygen-sensitive activation of evofosfamide depends on one-electron reduction, yet the reductases that catalyse this process in tumours are unknown. We used RNA sequencing, whole-genome CRISPR knockout and reductase-focused shRNA screens to interrogate modifiers of evofosfamide activation in cancer cell lines. Involvement of mitochondrial electron transport in the activation of evofosfamide and the related nitroaromatic compounds EF5 and FSL-61 was investigated using 143B ρ^0 (rho zero) cells devoid of mitochondrial DNA and biochemical assays in UT-SCC-74B cells. The potency of evofosfamide in 30 genetically diverse cancer cell lines correlated with the expression of genes involved in mitochondrial electron transfer. A whole-genome CRISPR screen in KBM-7 cells identified the DNA damage response factors *SLX4IP*, *C10orf90* (*FATS*) and *SLFN11*, in addition to the key regulator of mitochondrial function *YME1L1* and several complex I constituents as modifiers of evofosfamide sensitivity. A reductase-focused shRNA screen in UT-SCC-74B cells similarly identified mitochondrial respiratory chain factors. Surprisingly, 143B ρ^0 cells showed enhanced evofosfamide activation and sensitivity but had global transcriptional changes including increased expression of non-mitochondrial flavoreductases. In UT-SCC-74B cells, evofosfamide oxidised cytochromes *a*, *b* and *c* and inhibited respiration at complexes I, II and IV without quenching ROS production. Our results suggest that the mitochondrial electron transport chain contributes to evofosfamide activation and that predicting evofosfamide sensitivity in patients by measuring the expression of canonical bioreductive enzymes such as P450 oxidoreductase (POR) is likely to be futile.

Molecular Pharmacology Fast Forward. Published on April 12, 2019 as DOI: 10.1124/mol.118.115196
This article has not been copyedited and formatted. The final version may differ from this version.

Introduction

Hypoxia has been pursued as an oncology target due to its severity in tumours and its roles in cancer progression and therapy resistance (Wilson and Hay, 2011). The latter reflects the central role of O_2 in the conversion of radiation-induced DNA radicals to strand breaks, in addition to extensive evidence that hypoxic regions are refractory to systemic cytotoxic and immune therapies (Trédan *et al.*, 2007; Chouaib *et al.*, 2017). One strategy for targeting hypoxia involves the use of prodrugs that undergo reductive activation that is suppressed by molecular oxygen. The leading example of this class, evofosfamide (TH-302), is a *bis*-alkylating bromo-*iso*-phosphoramide mustard (Br-IPM) deactivated by a bioreductive 2-nitroimidazole trigger (Duan *et al.*, 2008). One-electron reduction of evofosfamide produces a radical anion that rapidly fragments to release Br-IPM (Meng *et al.*, 2012), which in turn undergoes halide exchange to produce a second DNA crosslinking agent, Cl-IPM (Hong *et al.*, 2018). In the presence of O_2, the prodrug radical is oxidised, thus conferring hypoxia selectivity (Fig. 1A).

Evofosfamide has been extensively tested in preclinical models, where it shows hypoxia-dependent monotherapy activity (Sun *et al.*, 2012) and augments the efficacy of approved therapies including radiation (Peeters *et al.*, 2015; Lohse *et al.*, 2016; Jamieson *et al.*, 2018; Takakusagi *et al.*, 2018), immune checkpoint blockade (Jamieson *et al.*, 2018; Jayaprakash *et al.*, 2018), bortezomib (Hu *et al.*, 2013), mTOR inhibitors (Sun *et al.*, 2015), transarterial chemoembolisation (Duran *et al.*, 2017) and various cytotoxic agents (Liu *et al.*, 2012; Zhang *et al.*, 2016; Haynes *et al.*, 2018). Clinically, evofosfamide is well-tolerated (Weiss *et al.*, 2011) and was active in combination with gemcitabine for advanced pancreatic cancer (Borad *et al.*, 2015) and doxorubicin for soft-tissue sarcoma (Chawla *et al.*, 2014) in phase II randomised and single-arm studies, respectively. Disappointingly, definitive trials in both indications were

Molecular Pharmacology Fast Forward. Published on April 12, 2019 as DOI: 10.1124/mol.118.115196
This article has not been copyedited and formatted. The final version may differ from this version.

negative for overall survival benefit in patients not selected for tumour hypoxia (Cutsem *et al.*, 2016; Tap *et al.*, 2017). While the negative SARC021 result may in part reflect chemical antagonism between evofosfamide and doxorubicin (Anderson *et al.*, 2017), the narrow shortfall in primary endpoint in the MAESTRO pancreatic cancer study has been attributed to diminished prodrug exposures caused by a formulation change (Higgins *et al.*, 2018) and lack of predictive biomarkers (Domenyuk *et al.*, 2018). Reflecting the key role of hypoxia in immune suppression, evofosfamide is currently being evaluated in combination with ipilimumab for solid tumours in a phase IB study (NCT03098160).

Since reductive activation of evofosfamide is required for anti-tumour activity, profiling the enzymes that catalyse this reaction is potentially an important aspect of predictive biomarker strategies. As for other prodrugs that depend on initial one-electron reduction, the activation of evofosfamide is inhibited by diphenyleneiodonium, indicating catalysis by FMN- and FAD-dependent flavoproteins that mediate one-electron transfer from NAD(P)H to substrates (Meng *et al.*, 2012). While P450 oxidoreductase (POR) (Hunter *et al.*, 2012; Meng *et al.*, 2012) and FAD-dependent oxidoreductase domain containing 2 (FOXRED2) (Hunter, Jaiswal, *et al.*, 2014) have been shown to activate evofosfamide when expressed at supra-physiological levels, knockdown or knockout of *POR* in cell lines causes little or no decrease in evofosfamide cytotoxicity under hypoxia (Su, Gu, *et al.*, 2013; Hunter *et al.*, 2015; Hong *et al.*, 2018). Moreover, the promiscuity and redundancy of flavoreductases as xenobiotic metabolising enzymes has obstructed identification of the proteins that activate evofosfamide in tumours. Here, we use integrated functional CRISPR and shRNA screens and gene expression analysis to interrogate genetic modifiers of evofosfamide activity. We present evidence for a role of mitochondrial electron transport in the reductive activation of evofosfamide, with implications for the utility of reductase profiling in the use of this agent for precision cancer medicine.

Molecular Pharmacology Fast Forward. Published on April 12, 2019 as DOI: 10.1124/mol.118.115196
This article has not been copyedited and formatted. The final version may differ from this version.

Materials and Methods

Compounds. Evofosfamide was gifted by Threshold Pharmaceuticals (South San Francisco, CA). PR-104A, SN30000 and deuterated standards for evofosfamide metabolism assays were synthesised at the Auckland Cancer Society Research Centre (Auckland, New Zealand). The purity of compounds (>95%) was assessed by HPLC and DMSO stock solutions stored at –80°C.

Cell lines and Culture. 786-O, A375, A549, ACHN, BxPC-3, Caki-1, Calu-6, DU 145, H460, H82, HCT 116, Hs766T, HT-1080, HT-29, IGROV-1, KHOS/NP, LNCaP, Malme-3M, MDA-MB-231, MIA PaCa-2, PANC-1, PC-3, PLC/PRF/5, RPMI 8226, SiHa, SK-BR-3, SK-MEL-2, SK-MEL-28, SK-MEL-5, SU.86.86, T-47D and U-87 MG cell lines were sourced as reported (Meng *et al.*, 2012) and cultured as recommended by the American Type Culture Collection (Manassas, VA). KBM-7 cells were procured from Haplogen (Vienna, Austria) and cultured in IMDM + 5% FCS. UT-SCC-74B cells were gifted by Prof. Reidar Grénman (University of Turku, Finland) and cultured in MEM + 10% FCS, 4.5 $mg.mL^{-1}$ D-glucose, 1.9 $mg.mL^{-1}$ sodium bicarbonate, 1 mM sodium pyruvate and 20 mM HEPES. 143B ρ^0 and parental 143B cells were gifted by Prof. Mike Berridge (Malaghan Institute, Wellington, New Zealand) and cultured in MEM + 10% FCS, 3.5 $mg.mL^{-1}$ D-glucose, 20 mM HEPES, 1 mM sodium pyruvate, and 50 $\mu g.mL^{-1}$ uridine. Rho zero status was confirmed by PCR using the *MT-TL1* primers GAT-GGC-AGA-GCC-CGG-TAA-TCG-C and TAA-GCA-TTA-GGA-ATG-CCA-TTG-CG and the *GAPDH* primers ACG-GGA-AGC-TTG-TCA-TCA-AT and TGG-ACT-CCA-CGA-CGT-ACT-CA. All cell lines were propagated from cryopreserved vials authenticated by short-tandem repeat analysis and confirmed to be mycoplasma-free by PlasmoTest (InvivoGen, San Diego, CA).

Molecular Pharmacology Fast Forward. Published on April 12, 2019 as DOI: 10.1124/mol.118.115196
This article has not been copyedited and formatted. The final version may differ from this version.

Antiproliferative (IC_{50}) Assays. The sensitivity of cell lines to drugs was assessed by antiproliferative (IC_{50}) assay. For the cancer cell line panel (Fig. 1), 2,000 cells were seeded in 0.5 mL per well in 24-well plates and allowed to attach over 24 h. The plates were then placed under anoxia (<10 ppm gas-phase O_2) inside an H_2-scrubbed glove port chamber (Hypoxystation) and the medium exchanged with pre-equilibrated anoxic medium containing a dilution series of evofosfamide. Cells were exposed to evofosfamide over 2 h, then drug washed out by two medium changes. Parallel plates were challenged with evofosfamide under 20% O_2. The cells were cultured for 7 d prior to assessing viability using alamarBlue (Thermo Fisher Scientific; Waltham, MA). For the 143B and ρ^0 lines, 300 or 800 cells, respectively, were seeded in 0.1 mL per well in 96-well plates under anoxia (Coy anaerobic chamber) and allowed to attach over 2 h. Drugs were then added to the plates in dilution series and exposed over 4 h. Parallel plates were challenged under 20% O_2. Drug washout was effected by three medium changes and the plates were then incubated for 5 d prior to assessing culture density by sulphorhodamine B staining. In both cases, four-parameter variable slope functions were fitted to the concentration-response data using least squares and solved to define the drug concentrations for 50% inhibition of cell growth relative to vehicle-treated control wells on the same plate. The parameters in these functions (Hill slope, EC_{50}, minimum and maximum response) were unconstrained. IC_{50} data are presented as the mean ± SEM for ≥3 independent experiments per cell line. Hypoxic selectivity was quantified as the ratio of mean IC_{50} values under normoxia and anoxia.

Evofosfamide Metabolism Assays. Reductive activation of evofosfamide in cell lines was assessed by liquid chromatography-tandem mass spectrometry as the concentrations of Br-IPM, Cl-IPM and Tr-H metabolites produced in anoxic cell cultures exposed to 30 μM

Molecular Pharmacology Fast Forward. Published on April 12, 2019 as DOI: 10.1124/mol.118.115196
This article has not been copyedited and formatted. The final version may differ from this version.

evofosfamide for 1 h. Metabolite concentrations in the intra- and extracellular fractions were measured separately then summed for statistical analysis. The cell culture and bioanalytical methods have been reported in detail (Hong *et al.*, 2018).

RNA Sequencing. RNA sequencing (RNAseq) data for the cancer cell line panel were retrieved from the Cancer Cell Line Encyclopedia. For 143B and ρ^0 cells, RNA was extracted from cultures in logarithmic growth (*n*=3 independent cultures per line) and stranded mRNA libraries generated using a NEXTflex Rapid Directional kit (Perkin Elmer; Waltham, MA) with v4 chemistry. Final libraries were quantified using a Qubit high-sensitivity DNA Assay Kit (Thermo Fisher Scientific; Waltham, MA) and quality was assessed with a TapeStation 4200 (Agilent; Santa Clara, CA). Libraries were normalised, pooled equimolarly and sequenced on a NextSeq500 using a 75 bp single-end flow cell (Illumina; San Diego, CA). Reads were aligned to hg19 with STAR and mRNA abundance estimated using RSEM. For both datasets, expected counts were $\log_2$ transformed and quantile normalised before analysis. Differential expression analysis, correlation with IC_{50} data and hierarchical clustering were performed in R and used the *limma*, Pearson and ward.D methods with Euclidean distance. Statistical enrichment of gene ontology (GO) and pathway classifications among gene lists was assessed using GeneSetDB (genesetdb.auckland.ac.nz).

Whole-Genome CRISPR Knockout Screen. KBM-7 cells were stably transduced with *Streptococcus pyogenes* Cas9 (lentiCas9-Blast vector) at an MOI of 0.02 and expression confirmed by immunoblotting (mouse anti-Cas9 monoclonal antibody clone 7A9 diluted 1:1000; Diagenode, Belgium). The resulting pool was transduced with the GeCKOv2 single guide RNA (sgRNA) library (lentiGuide-Puro vector) at an MOI of 0.25 and selected in puromycin for 7 d. Triplicate cultures of 10^8 cells (i.e. 810 cells per sgRNA in the GeCKOv2

Molecular Pharmacology Fast Forward. Published on April 12, 2019 as DOI: 10.1124/mol.118.115196
This article has not been copyedited and formatted. The final version may differ from this version.

library) were exposed to 0.013 μM evofosfamide as stirred suspensions (10^6 cells.mL^{-1}) for 1 h under anoxia (Hypoxystation; Don Whitley Scientific), with a prior 30-min drug-free incubation to deplete O_2. Evofosfamide was removed by centrifugation and the cultures maintained under 20% O_2 with daily assessment of regrowth (Coulter particle counter). Two cycles of drug challenge were imposed. Triplicate vehicle-treated cultures were exposed to anoxia without evofosfamide and maintained in parallel. Genomic DNA was isolated from cells at screen endpoint (day 26) using QIAamp DNA Blood Maxi kits (Qiagen; Hilden, Germany) and sgRNA sequences PCR-amplified as described (Sanjana *et al.*, 2014). Sequencing was performed on a NextSeq500 (Illumina; San Diego, CA) using a high-output, 150 bp paired-end flow cell. The screens were deconvolved and statistical significance of sgRNA enrichment or depletion in evofosfamide-treated cultures relative to controls was assessed using the MAGeCK (sourceforge.net/p/mageck) and PinAPL-Py (pinapl-py.ucsd.edu) algorithms. Genes that were enriched or depleted at a statistical significance threshold of $P<0.005$ according to one or both algorithms were considered of interest.

Reductase-Focused shRNA Screen. UT-SCC-74B cells were transduced at an MOI of 0.38 with a previously-reported (Hunter *et al.*, 2015) custom pool of 1,821 shRNA constructs (pLKO.1 vector) targeting 359 genes enriched for oxidoreductases and covering the annotated human flavoproteome. Triplicate transduced cultures, each of 150×10^6 cells, were treated with 0.75 μM evofosfamide as stirred single-cell suspensions (10^6 cells.mL^{-1}) for 1 h under anoxia and subsequently regrown under 20% O_2. Triplicate, vehicle-treated control cultures were maintained in parallel. Cells were seeded for assessment of plating efficiency immediately prior to and following evofosfamide challenge and at screen endpoint (i.e. complete recovery evident 18 d after treatment by phase-contrast microscopy). Genomic DNA was extracted from cells and shRNA barcodes PCR-amplified, sequenced and scored as reported (Hunter *et al.*, 2015).

Molecular Pharmacology Fast Forward. Published on April 12, 2019 as DOI: 10.1124/mol.118.115196
This article has not been copyedited and formatted. The final version may differ from this version.

Statistical significance of shRNA enrichment in evofosfamide-treated cultures relative to controls was assessed using the MAGeCK and RIGER methods.

FSL-61 Metabolism Assays. Reductive activation of the fluorogenic probe FSL-61 was measured as described (Su, Guise, *et al.*, 2013). Briefly, anoxic cell suspensions (2×10^6.mL^{-1}) in Phenol Red-free medium were labelled with 300 or 600 μM FSL-61 for 3 h then analysed using a BD Accuri C6 flow cytometer with excitation and emission wavelengths of 355 and 425-475 nm, respectively. The distributions of fluorescence area events for ρ^0 and 143B cells were compared to cells not labelled with FSL-61 but otherwise handled identically.

EF5 Metabolism Assays. EF5 binding was assayed as described (Wang *et al.*, 2012) with modifications. Briefly, 10^6 cells were pre-incubated under anoxic conditions in 10 mL Phenol Red-free MEMα with 5% FCS for 30 min with continuous stirring before being exposed to 120 μM EF5 for 2 h. Cells were then centrifuged (1000 × *g*, 5 min) and fixed in cold 4% paraformaldehyde for 1 h. The fixed cells were incubated in blocking buffer (PBST with 20% low-fat milk, 1.5% lipid-free albumin and 5% mouse serum) at 4°C for 30 min then stained overnight at 4°C with 100 μg.mL^{-1} Alexa488-conjugated anti-EF5 antibody (supplied by Prof. Cameron Koch, University of Pennsylvania, PA). Samples were washed twice with PBST and once with PBS then analysed using BD Accuri C6 or BD LSR II flow cytometers.

Cellular Physiology Assays. Mitochondrial respiration and ROS production were assessed using OROBOROS™ oxygraphs (O2k; Innsbruck, Austria) and analysed in real time with DatLab 7.1 software after instrument calibration and back-flux correction. Substrate−inhibitor−uncoupler protocols were employed to deconvolute the characteristics of the mitochondrial electron transport system components. Cells (5×10^6 in 2 mL) were

Molecular Pharmacology Fast Forward. Published on April 12, 2019 as DOI: 10.1124/mol.118.115196
This article has not been copyedited and formatted. The final version may differ from this version.

introduced in the O2k chamber containing fully-aerated PBS at 37ºC. After signal stabilisation, permeabilisation was effected by titrating digitonin to 10 µg/10^6 cells. Respiratory substrates were then added at saturation (5 mM pyruvate, 2.5 mM malate, 10 mM glutamate, 10 mM succinate and 2.5 mM ADP) to achieve OXPHOS state (maximum respiration attributed to oxidative phosphorylation). Evofosfamide (0-200 µM) or vehicle (DMSO equivalent volume) were titrated on permeabilised cells at OXPHOS state. The maximum contribution of succinate dehydrogenase (complex II) to OXPHOS was determined with the addition of the complex I inhibitor rotenone (0.5 µM). Respiration not efficiently directed to OXPHOS but dissipated to proton leak (LEAK) was determined with the addition of the ATP F0F1 synthase inhibitor oligomycin (2 µg.mL^{-1}) on cells at OXPHOS state. The maximum activity of cytochrome *c* oxidase (complex IV) was measured with *N*,*N*,*N′*,*N′*-tetramethyl-*p*-phenylenediamine (TMPD, 0.5 mM) and ascorbate (2 mM) to protect against TMPD auto-oxidation. Potassium cyanide (1 mM) was added at the end of respirometry assays to (determine TMPD auto-oxidation and induce the maximal reductive state of mitochondrial cytochromes.

ROS production was assessed concurrently with respiration by Amplex UltraRed assay as previously described (Pham *et al.*, 2014). Cytochrome spectra were also obtained simultaneously using purpose-build light-emitting diodes (370-750 nm) placed adjacent to the O2k chamber. Reflected light was collected via a 1 mm optic fibre connected to a USB4000 spectrophotometer (Ocean Optics, Inc.). Absorbance was measured with SpectraSuite 2.0.162. The change in absorption mediated by evofosfamide was obtained by reference to the absorption spectra prior to drug titration at OXPHOS state. The relative contribution of each cytochrome (*a*, *b* and *c*) to the absorbance was determined using their respective extinction coefficients. Normalisation of spectra was made using KCN to maximally reduce mitochondrial cytochromes.

Molecular Pharmacology Fast Forward. Published on April 12, 2019 as DOI: 10.1124/mol.118.115196
This article has not been copyedited and formatted. The final version may differ from this version.

Statistics. Statistical tests were performed in R, Python or GraphPad Prism v7 and were two-tailed where applicable. The specific tests used, the number of experimental replicates and representations of dispersion and central tendency are described in figure legends. Protein-protein interaction networks were defined using the STRING database (string-db.org), while overrepresentation of GO terms in gene lists was assessed using PANTHER (pantherdb.org), DAVID (david.ncifcrf.gov) and GeneSetDB (genesetdb.auckland.ac.nz). $P<0.05$ is denoted as '*', $P<0.01$ as '**' and $P<0.001$ as '***'.

Molecular Pharmacology Fast Forward. Published on April 12, 2019 as DOI: 10.1124/mol.118.115196
This article has not been copyedited and formatted. The final version may differ from this version.

Results

Evofosfamide Sensitivity Correlates with Expression of Mitochondrial Genes in Cancer Cell Lines. To investigate sources of variation in the sensitivity of cancer cells to evofosfamide, IC_{50} was measured under anoxia ("N_2") and normoxia ("air") in a panel of 32 histologically-diverse cell lines (Fig. 1B). Drug sensitivity data were then related to gene expression profiles from RNAseq. This IC_{50} study recapitulated a prior dataset in the same panel (Meng *et al.*, 2012), except that a longer regrowth endpoint was used (7-d vs 3-d) to more closely reflect clonogenic survival than acute antiproliferative effects. Evofosfamide showed low-micromolar potency under anoxia with a 67-fold range in IC_{50} values − less than the 900-fold range observed using the 3-d endpoint (Meng *et al.*, 2012). The two datasets were generally well-correlated with the exception of Hs766T and IGROV-1, which were markedly more sensitive to evofosfamide than in the 3-d assay (Fig. 1C). The prodrug was strongly inactivated by ambient O_2, conferring a median Air−N_2 IC_{50} ratio of 48 (range 16-260; Fig. 1B), while the patterns of sensitivity were highly correlated under both conditions (Supplemental Fig. 1A). To explore biological determinants of evofosfamide sensitivity, RNAseq data available from the Cancer Cell Line Encyclopedia for 30 of the cell lines (Fig. 2A) were correlated with IC_{50} measures. The 173 genes with expression values that inversely correlated with evofosfamide IC_{50} under anoxia ($R \leq -0.4$) were overrepresented for GO annotations relating to mitochondrial localisation and function (Table 1, Supplemental Fig. 2). To assess the extent to which a signature derived from these genes might associate with evofosfamide sensitivity, we computed the first principal component (PC1) of expression values for these genes and identified a quantitative association between the rank order of cell lines by PC1 and evofosfamide sensitivity (Fig. 2B). Moreover, dichotomising the cell line panel by the PC1 median defined groups with significantly different drug sensitivity distributions (Supplemental Fig. 1B).

Molecular Pharmacology Fast Forward. Published on April 12, 2019 as DOI: 10.1124/mol.118.115196
This article has not been copyedited and formatted. The final version may differ from this version.

Network analysis of the correlating genes revealed an interacting cluster with annotations relating mitochondrial inner membrane localisation, mitochondrial protein biosynthesis, electron transport and metabolism (Fig. 2C).

Whole-genome CRISPR Knockout and Reductase-Focused shRNA Screens Identify Mitochondrial Involvement in Evofosfamide Activity. As an orthogonal line of investigation, a genome-scale CRISPR knockout screen was performed in near-haploid KBM-7 cells transduced with the GeCKOv2 sgRNA library (Fig. 3A). Two treatments with 0.013 μM evofosfamide under anoxia, which was the measured IC_{40} in KBM-7 (Supplemental Fig. 3), on days 0 and 7 inhibited total population growth by a factor of 10^4 relative to vehicle-treated cultures at screen termination (Fig. 3B). Evofosfamide-challenged cells acquired bulk resistance to the agent relative to drug-naïve cultures, with a dose-modifying factor (DMF) of 1.6 (Fig. 3C). The screen was deconvolved using the MAGeCK (sourceforge.net/p/mageck/) and PinAPL-Py (http://pinapl-py.ucsd.edu/) algorithms to identify sgRNA enriched or depleted by evofosfamide treatment and to aggregate the multiple guides specific for each gene to output a gene level score. as Among the most significant hits in the screen were the mitochondrial factor *YME1L1* and the DNA damage response and repair factors *C10orf90* (*FATS*), *SLX4IP* (*C20orf94*) and *SLFN11* (Fig. 3D-E). Considering all sgRNA targets positively selected by evofosfamide (i.e. sgRNA representation increased following drug challenge; $P<0.005$ by MAGeCK, PinAPL-Py or both, Fig. 3E) defined a gene list overrepresented in GO terms relating to mitochondrial respiration and electron transfer from NADH to ubiquinone (Table 2). Among these positively selected sgRNA targets was an interacting protein network encompassing subunits and regulators of mitochondrial respiratory complex I (Fig. 3F).

Molecular Pharmacology Fast Forward. Published on April 12, 2019 as DOI: 10.1124/mol.118.115196
This article has not been copyedited and formatted. The final version may differ from this version.

A parallel screen was performed in the lingual squamous cell carcinoma line UT-SCC-74B using a previously-reported custom pool of 1,821 shRNA targeting 359 genes, including the majority of annotated human flavoproteins (Hunter *et al.*, 2015). This screen was analogous to the KBM-7 study (Fig. 3A), except that a single instance of acute evofosfamide treatment was imposed, resulting in three logs of clonogenic cell killing (Fig. 4A). Deconvoluting the screen identified factors putatively involved in sensitivity to evofosfamide, including constituents of mitochondrial complexes I and III (Fig. 4B). The resulting list of candidate genes was overrepresented for GO annotations relating to mitochondrial localisation and respiratory electron transport, even after correcting for the reductase-enriched target-space of the shRNA pool (Table 3). The full list of positively-selected shRNA targets (P<0.05 by MAGeCK, RIGER or PinAPL-Py) encompassed a cluster of interacting proteins functioning in mitochondrial electron transport (Fig. 4C).

Rho Zero Cells Demonstrate Enhanced Reductive Metabolism of Bioreductive Prodrugs and Global Transcriptional Changes. Mitochondrial involvement in the reductive activation of evofosfamide was investigated in rho zero (ρ^0) cells derived from the 143B osteosarcoma line by protracted treatment with ethidium bromide to deplete mitochondrial DNA (King and Attardi, 1989). Rho zero status was confirmed by PCR for mitochondrial DNA-encoded *MT-TL1* (Fig. 5A). Functionally, ρ^0cells showed profound loss of mitochondrial O_2 flux in the OXPHOS, CII, LEAK and CIV states (Fig. 5B). Despite lacking a functional respiratory transport chain, ρ^0 cells demonstrated elevated generation of the evofosfamide reduction metabolites Br-IPM, Cl-IPM and 2-nitroimidazole fragmentation product (1,5-dimethyl-2-nitroimidazole, 'Tr-H', Fig. 5C). Rho zero cells also showed elevated reductive activation of the fluorogenic 6-nitroquinolone FSL-61 (Su, Guise, *et al.*, 2013) and the bioreductive probe EF5, which shares a 2-nitroimidazole moiety with evofosfamide (Fig. 5D).

Rho zero cells were correspondingly more sensitive to evofosfamide and the additional hypoxia-activated prodrugs PR-104A and SN30000 specifically under anoxia (Fig. 5E), with a commensurate increase in selectivity (Supplemental Fig. 4). Given these surprising observations, gene expression features of the ρ^0 line were investigated by RNAseq. Relative to parental 143B cells, the ρ^0 line (all analysed in triplicate) showed widespread transcriptional changes encompassing a broad array of molecular pathways, with 6,741 transcripts differentially expressed beyond a Benjamini−Hochberg adjusted *P*-value of 0.05 (Fig. 6A). Notably, ρ^0 cells showed higher expression of genes with GO annotations relating to DNA repair (adjusted $p<10^{-7}$; Fig. 6B) but lower expression of genes with GO annotations relating to DNA damage response (*P*-value after adjusting for multiple comparisons <0.01; Fig. 6C). The expression of a number of flavoreductases, including the evofosfamide-activating enzyme P450 oxidoreductase (POR), was also higher in ρ^0 cells (Fig. 6D).

Evofosfamide Oxidises Mitochondrial Cytochromes and Inhibits Respiration. To directly examine the involvement of mitochondrial electron transport in evofosfamide reduction, key components of mitochondrial function were assessed in permeabilised UT-SCC-74B cells exposed to evofosfamide (5-200 µM). Shifts in absorption spectra confirmed the oxidation of mitochondrial cytochromes *a*, *b* and *c* by evofosfamide with a clear shift in the Soret band from 410 to 400 nm, characteristic of cytochrome *c* oxidation (Vanderkooi *et al.*, 1980) (Fig. 7A). All cytochromes appeared to be equally affected, with maximum oxidation reached at approximately 25 µM evofosfamide (Fig. 7B). Since components of the mitochondrial transport system were affected by the prodrug, the efficiency of electron transport to oxygen and electron leakage to ROS production were assessed concurrently. We thereby assessed whether reduction of evofosfamide by electron carriers in the transport chain would compete with leakage of electrons to generate superoxide, and hence H_2O_2. However,

Molecular Pharmacology Fast Forward. Published on April 12, 2019 as DOI: 10.1124/mol.118.115196
This article has not been copyedited and formatted. The final version may differ from this version.

electron capture by the prodrug did not appear to be sourced from mitochondrial ROS (Fig. 7C), but rather from respiration, which was inhibited by evofosfamide in a concentration-dependent manner (Fig. 7D). Respiration was equally affected in all mitochondrial respiration states, with specific respiration rates approximately halved in the presence of 200 µM evofosfamide relative to vehicle controls (Fig. 7E).

Molecular Pharmacology Fast Forward. Published on April 12, 2019 as DOI: 10.1124/mol.118.115196
This article has not been copyedited and formatted. The final version may differ from this version.

Discussion

Severe hypoxia is a prevalent and specific feature of the tumour microenvironment that contributes to aggressive and refractory disease (Wilson and Hay, 2011). Despite its strong rationale as a target, the most widely explored strategy for addressing tumour hypoxia – bioreductive prodrugs – has had a chequered clinical development history. Agents such as tirapazamine, evofosfamide, PR-104, apaziquone (EO9), banoxantrone (AQ4N) and tarloxotinib have each had trials (in some cases, major registrational studies) that either failed to meet efficacy or safety endpoints or were discontinued for commercial reasons. Recognised obstacles in the development of bioreductive prodrugs include toxicological interactions with standards of care (DiSilvestro *et al.*, 2014), stringent micropharmacokinetic requirements (Hicks *et al.*, 2003) and challenges in the application of diagnostic tools to select patients whose tumours express the target of these drugs (Hunter *et al.*, 2016). The target in question is multifactorial and encompasses both hypoxia and the intrinsic sensitivity of malignant cells to the active drug species. The principal challenge has been in clinically assessing hypoxia itself, as PET−CT imaging with nitroimidazole radiopharmaceuticals and analysis of hypoxia markers in tissue samples have been confounded by scalability and macroregional heterogeneity in tumour hypoxia, respectively. An example of intrinsic sensitivity is deficiency in homologous recombination repair of DNA double-strand breaks, which sensitises model tumours to prodrugs that release DNA crosslinking agents (Hunter, Hsu, *et al.*, 2014). Indeed, the present study identified sgRNA targeted to *SLX4IP* (*C20orf94*) to be negatively selected by evofosfamide. SLX4IP forms a Holliday junction resolvase in complex with SLX4, ERCC4, ERCC1, MUS81, EME1 and SLX1 and thus has a putative role in DNA crosslink repair (Svendsen *et al.*, 2009). The gene is frequently mutated in paediatric acute lymphoblastic leukaemia (Meissner *et al.*, 2010), suggesting that these neoplasms may be sensitive to

Molecular Pharmacology Fast Forward. Published on April 12, 2019 as DOI: 10.1124/mol.118.115196
This article has not been copyedited and formatted. The final version may differ from this version.

evofosfamide. Similarly, positive selection of sgRNA targeting *C10orf90* (*FATS*) and *SLFN11* by evofosfamide is consistent with the function of these genes in DNA damage response (Zoppoli *et al.*, 2012; Smurnyy *et al.*, 2014) and platinum sensitivity (Tian *et al.*, 2012; Nogales *et al.*, 2015).

Another aspect of the bioreductive prodrug target is the facility of prodrug activation given a state of hypoxia, i.e. the bioreductive capacity of the hypoxic cancer cell. Accordingly, identifying the reductases responsible for prodrug activation has been the subject of substantial effort, with the ultimate goal of profiling their expression in tumours to aid in predicting sensitivity. Prodrugs that require initial one-electron reduction are activated by flavoproteins, a family of approximately 100 oxidoreductases that catalyse electron transfer from NAD(P)H via FMN and FAD to substrates. Candidate-based screening of subsets of these enzymes by overexpression in cell lines has identified POR, MTRR, NDOR1, NOS2A, FOXRED2 and CYB5R3 as capable of prodrug metabolism (Patterson *et al.*, 1997; Papadopoulou *et al.*, 2003; Guise *et al.*, 2007, 2012; Chandor *et al.*, 2008; Hunter, Jaiswal, *et al.*, 2014; Wang *et al.*, 2015). In the case of evofosfamide, this has only been demonstrated for POR and FOXRED2 (Hunter *et al.*, 2012; Meng *et al.*, 2012; Hunter, Jaiswal, *et al.*, 2014). However, flavoreductases are promiscuous in their xenobiotic metabolism, and the more relevant question is the complement of enzymes actually responsible for prodrug activation in tumours at native expression levels. This calls for correlative or high-throughput, loss-of-function discovery approaches. Using gene expression analysis, functional CRISPR and shRNA screens, we present evidence for the mitochondrial electron transport chain (ETC)as a key source of reducing equivalents in the activation of evofosfamide, where several flavoproteins serve as constituents of complexes in the electron transport chain (ETC). While the actual electron donors are not identified in this study (and could be flavoproteins, cytochromes or Fe-S centres), the cell physiological data

Molecular Pharmacology Fast Forward. Published on April 12, 2019 as DOI: 10.1124/mol.118.115196
This article has not been copyedited and formatted. The final version may differ from this version.

presented are consistent with evofosfamide intercepting electrons at multiple nodes of the ETC (Fig. 7F). Although we note that there is a limited precedent for mitochondrial reduction of nitro compounds (Köchli *et al.*, 1980; Bironaite *et al.*, 1991), this represents a conceptually new model of the reductive activation of evofosfamide. While the oxidation of all cytochromes was affected by the prodrug, respiratory data suggested that complex II negligibly contributes to respiration (i.e. only marginally fuels the mitochondrial transport system with electrons) in the UT-SCC-74B model investigated and that the overall effect of the prodrug is primarily mediated by the decrease in electron transport prior to complex III (containing cytochrome *b*). This is evidenced by the fact that all components with the exception of complex I and the ubiquinone pool were affected independently of mitochondrial state. Interestingly, although not explicitly investigated here, the model suggests a possible mechanism of hypoxia selectivity (in addition to oxidation of the prodrug radical by O_2) as ETC redox centres are fully reduced under hypoxia due to the absence of O_2 as terminal electron acceptor. Our model also implies that the increased activity of evofosfamide in tumour models conferred by pre-treatment with pyruvate (Takakusagi *et al.*, 2014) may reflect enhanced mitochondrial electron flux (and thus prodrug activation) in addition to enhancing hypoxia through oxygen consumption. Similarly, our observation that evofosfamide inhibits cellular respiration implies that this prodrug may decrease tumour hypoxia both by direct ablation of hypoxic regions and by suppressing oxygen consumption, contributing to its efficacy in combination with radiotherapy that we and others have reported (Nytko *et al.*, 2017; Jamieson *et al.*, 2018; Takakusagi *et al.*, 2018).

It is notable that the mitochondrial signature we observed in the present study, which spanned multiple cancer cell lineages, contrasts with the proliferation signature that we previously observed to associate with evofosfamide sensitivity specifically in human papillomavirus-negative head and neck squamous cell carcinoma (Jamieson *et al.*, 2018). This

distinction may arise from the fact that rates of evofosfamide activation were more homogeneous in models of the latter indication, with evofosfamide sensitivity principally determined by cellular phenotypes downstream of prodrug activation.

Curiously, we found mitochondria-deficient 143B ρ^0 cells to show enhanced activation of evofosfamide and other prodrugs, although massive transcriptional reprogramming in these cells – which included upregulation of a number of non-mitochondrial flavoreductases such as *POR* – suggests that these cells are far from an isogenic system and have limited utility in dissecting the contribution of mitochondria to bioreductive prodrug activation. Nonetheless, the observation underscores the view that mitochondrial electron transport is not the sole source of evofosfamide reduction. Indeed, ρ^0 cells have been reported to show increased cytosolic NADH/NAD^+ and NADPH/$NADP^+$ ratios (Naviaux, 2008), which would be consistent with enhanced electron flux via non-mitochondrial NAD(P)H-dependent flavoreductases. Of interest, ρ^0 cells have been reported to show altered one-carbon metabolism, with increased S-adenosyl methionine synthesis and consequent epigenetic silencing via CpG methylation (Smiraglia *et al.*, 2008). This may be one mechanism for the transcriptional reprogramming we observed.

If the mitochondrial ETC plays a significant role in tumour activation of evofosfamide, differences in mitochondrial biology between malignancies may be a contributor to evofosfamide sensitivity. Warburg's original contention that the fundamental lesion in cancer cells is mitochondrial dysfunction is no longer accepted, but mitochondrial changes are common in many tumours and mitochondrial DNA copy number and mass vary widely (Vyas *et al.*, 2016). In addition, hypoxia modulates mitochondrial function through multiple mechanisms including HIF-1-dependent transcription of pyruvate dehydrogenase kinase 1

Molecular Pharmacology Fast Forward. Published on April 12, 2019 as DOI: 10.1124/mol.118.115196
This article has not been copyedited and formatted. The final version may differ from this version.

(PDK1), which inhibits pyruvate dehydrogenase and thereby mitochondrial O_2 consumption (Kim *et al.*, 2006; Papandreou *et al.*, 2006). Thus, suppressed ETC flux in the hypoxic cells that evofosfamide seeks to target could compromise its metabolic activation, although under severe hypoxia lack of O_2 as the terminal electron acceptor could favour competing reduction of the prodrug.

A notable feature of our study was the absence of canonical prodrug reductases among the genes identified in the screens, with *POR* only modestly selected in the CRISPR screen (MAGeCK P=0.004; median increase in depth-normalised sgRNA read counts 1.7-fold) and completely absent in the shRNA screen. This contrasts with our earlier study, which utilised the same shRNA library to identify POR as the predominant activating reductase and a major sensitivity determinant for the benzotriazine di-*N*-oxide SN30000 (Hunter *et al.*, 2015). Our data suggest a minor role at most for POR in evofosfamide activation and provide further evidence for the view that the complement of activating enzymes is non-identical for different classes of prodrugs (Su, Gu, *et al.*, 2013), even if the sum bioreductive metabolism of chemically-distinct pharmacophores can be correlated across tumour models (Wang *et al.*, 2012). These findings, our description of involvement of mitochondrial electron transport in the reduction of evofosfamide and the curious enhanced sensitivity of rho zero cells to the same highlight the pleiotropic mechanisms of bioreductive prodrug activation. Moreover, they suggest that attempts to predict the facility of evofosfamide in tumours by measuring the expression of one or several reductases is likely to prove futile for patient stratification. Indeed, as we have advanced previously (Wang *et al.*, 2012; Hunter *et al.*, 2016), use of diagnostic 2-nitroimidazole probes such as EF5 that are activated by the same complement of reductases may be the only tractable means of predicting activation facility. Alternatively, biomarker strategies that focus on robustly stratifying patients according to tumour hypoxia may be more

Molecular Pharmacology Fast Forward. Published on April 12, 2019 as DOI: 10.1124/mol.118.115196
This article has not been copyedited and formatted. The final version may differ from this version.

successful. Nonetheless, it will be of interest to investigate mitochondrial involvement in the activation of other hypoxia-activated prodrugs and more broadly in the metabolism of nitro compounds, quinones and other xenobiotics with high one-electron reduction potentials.

Molecular Pharmacology Fast Forward. Published on April 12, 2019 as DOI: 10.1124/mol.118.115196
This article has not been copyedited and formatted. The final version may differ from this version.

Acknowledgements

The authors are grateful to Susan Pullen for assistance with IC_{50} assays, Dan Li for assistance with PCR, Dr Benjamin Dickson for the synthesis of deuterated internal standards and Dr Michael Hay for the synthesis of SN30000.

Molecular Pharmacology Fast Forward. Published on April 12, 2019 as DOI: 10.1124/mol.118.115196
This article has not been copyedited and formatted. The final version may differ from this version.

Authorship Contributions

Conducted experiments: Hunter, Devaux, Meng, Hong, Khan, Ketela, Sharma, Kakadia, Marastoni, Shalev.

Performed data analysis: Hunter, Devaux, Meng, Hong, Ketela.

Performed bioinformatic analyses: Hunter, Tsai, Print, Bohlander.

Participated in research study design: Hunter, Hickey, Print, Bohlander, Hart, Wouters, Wilson.

Wrote or contributed to writing the manuscript: Hunter, Devaux, Meng, Hong, Khan, Tsai, Ketela, Sharma, Kakadia, Marastoni, Shalev, Hickey, Print, Bohlander, Hart, Wouters, Wilson.

Molecular Pharmacology Fast Forward. Published on April 12, 2019 as DOI: 10.1124/mol.118.115196
This article has not been copyedited and formatted. The final version may differ from this version.

References

Anderson RF, Li D, and Hunter FW (2017) Antagonism in effectiveness of evofosfamide and doxorubicin through intermolecular electron transfer. *Free Radic Biol Med* **113**:564–570.

Bironaite DA, Čenas NK, and Kulys JJ (1991) The rotenone-insensitive reduction of quinones and nitrocompounds by mitochondrial NADH:ubiquinone reductase. *Biochim Biophys Acta - Bioenerg* **1060**:203–209.

Borad MJ, Reddy SG, Bahary N, Uronis HE, Sigal D, Cohn AL, Schelman WR, Stephenson J, Chiorean EG, Rosen PJ, Ulrich B, Dragovich T, Del Prete SA, Rarick M, Eng C, Kroll S, and Ryan DP (2015) Randomized phase II trial of gemcitabine plus TH-302 versus gemcitabine in patients with advanced pancreatic cancer. *J Clin Oncol* **33**:1475–1481.

Chandor A, Dijols S, Ramassamy B, Frapart Y, Mansuy D, Stuehr D, Helsby N, and Boucher J-L (2008) Metabolic activation of the antitumor drug 5-(Aziridin-1-yl)-2,4-dinitrobenzamide (CB1954) by NO synthases. *Chem Res Toxicol* **21**:836–843.

Chawla SP, Cranmer LD, Van Tine BA, Reed DR, Okuno SH, Butrynski JE, Adkins DR, Hendifar AE, Kroll S, and Ganjoo KN (2014) Phase II study of the safety and antitumor activity of the hypoxia-activated prodrug TH-302 in combination with doxorubicin in patients with advanced soft tissue sarcoma. *J Clin Oncol* **32**:3299–3306.

Chouaib S, Noman MZ, Kosmatopoulos K, and Curran MA (2017) Hypoxic stress: obstacles and opportunities for innovative immunotherapy of cancer. *Oncogene* **36**:439–445.

Cutsem E Van, Lenz H-J, Furuse J, Tabernero J, Heinemann V, Ioka T, Bazin I, Ueno M, Csõszi T, Wasan H, Melichar B, Karasek P, Macarulla TM, Guillen C, Kalinka-Warzocha E, Horvath Z, Prenen H, Schlichting M, Ibrahim A, and Bendell JC (2016) MAESTRO: A randomized, double-blind phase III study of evofosfamide (Evo) in combination with gemcitabine (Gem) in previously untreated patients (pts) with metastatic or locally advanced unresectable pancreatic ductal adenocarcinoma (PDAC). *J Clin Oncol* **34**:4007–4007.

DiSilvestro PA, Ali S, Craighead PS, Lucci JA, Lee YC, Cohn DE, Spirtos NM, Tewari KS, Muller C,

Gajewski WH, Steinhoff MM, and Monk BJ (2014) Phase III randomized trial of weekly cisplatin and irradiation versus cisplatin and tirapazamine and irradiation in stages IB2, IIA, IIB, IIIB, and IVA cervical carcinoma limited to the pelvis: A gynecologic oncology group study. *J Clin Oncol* **32**:458–464.

Domenyuk V, Magee D, Gatalica Z, Stark A, Kennedy P, Barker A, Berry DA, Poste GH, Halbert DD, Hart CP, Famulok M, Mayer G, Korn M, Miglarese MR, and Spetzler D (2018) Poly-ligand profiling (PLP) to differentiate pancreatic cancer patients who benefit from gemcitabine+evofosfamide versus gemcitabine+placebo treatment. *J Clin Oncol* **36**:12067.

Duan JX, Jiao H, Kaizerman J, Stanton T, Evans JW, Lan L, Lorente G, Banica M, Jung D, Wang J, Ma H, Li X, Yang Z, Hoffman RM, Ammons WS, Hart CP, and Matteucci M (2008) Potent and highly selective hypoxia-activated achiral phosphoramidate mustards as anticancer drugs. *J Med Chem* **51**:2412–2420.

Duran R, Mirpour S, Pekurovsky V, Ganapathy-Kanniappan S, Brayton CF, Cornish TC, Gorodetski B, Reyes J, Chapiro J, Schernthaner RE, Frangakis C, Lin M De, Sun JD, Hart CP, and Geschwind JF (2017) Preclinical benefit of hypoxia-activated intraarterial therapy with evofosfamide in liver cancer. *Clin Cancer Res* **23**:536–548.

Guise CP, Abbattista MR, Tipparaju SR, Lambie NK, Su J, Li D, Wilson WR, Dachs GU, and Patterson A V. (2012) Diflavin oxidoreductases activate the bioreductive prodrug PR-104A under hypoxia. *Mol Pharmacol* **81**:31–40.

Guise CP, Wang AT, Theil A, Bridewell DJ, Wilson WR, and Patterson A V. (2007) Identification of human reductases that activate the dinitrobenzamide mustard prodrug PR-104A: A role for NADPH:cytochrome P450 oxidoreductase under hypoxia. *Biochem Pharmacol* **74**:810–820.

Haynes J, McKee TD, Haller A, Wang Y, Leung C, Gendoo DMA, Lima-Fernandes E, Kreso A, Wolman R, Szentgyorgyi E, Vines DC, Haibe-Kains B, Wouters BG, Metser U, Jaffray DA, Smith M, and O'Brien CA (2018) Administration of hypoxia-activated prodrug evofosfamide after conventional adjuvant therapy enhances therapeutic outcome and targets cancer-initiating cells in preclinical models of colorectal cancer. *Clin Cancer Res* **24**:2116–2127.

Hicks KO, Pruijn FB, Sturman JR, Denny WA, and Wilson WR (2003) Multicellular resistance to

tirapazamine is due to restricted extravascular transport: A pharmacokinetic/pharmacodynamic study in HT29 multicellular layer cultures. *Cancer Res* **63**:5970–5977.

Higgins JP, Sarapa N, Kim J, and Poma E (2018) Unexpected pharmacokinetics of evofosfamide observed in phase III MAESTRO study. *J Clin Oncol* **36**:2568.

Hong CR, Dickson BD, Jaiswal JK, Pruijn FB, Hunter FW, Hay MP, Hicks KO, and Wilson WR (2018) Cellular pharmacology of evofosfamide (TH-302): A critical re-evaluation of its bystander effects. *Biochem Pharmacol* **156**:265–280.

Hu J, Van Valckenborgh E, Xu D, Menu E, De Raeve H, De Bryune E, Xu S, Van Camp B, Handisides D, Hart CP, and Vanderkerken K (2013) Synergistic induction of apoptosis in multiple myeloma cells by bortezomib and hypoxia-activated prodrug TH-302, in vivo and in vitro. *Mol Cancer Ther* **12**:1763–1773.

Hunter FW, Hsu H-L, Su J, Pullen SM, Wilson WR, and Wang J (2014) Dual targeting of hypoxia and homologous recombination repair dysfunction in triple-negative breast cancer. *Mol Cancer Ther* **13**:2501–2514.

Hunter FW, Jaiswal JK, Hurley DG, Liyanage HDS, McManaway SP, Gu Y, Richter S, Wang J, Tercel M, Print CG, Wilson WR, and Pruijn FB (2014) The flavoprotein FOXRED2 reductively activates nitro- chloromethylbenzindolines and other hypoxia-targeting prodrugs. *Biochem Pharmacol* **89**:224–235.

Hunter FW, Wang J, Patel R, Hsu HL, Hickey AJR, Hay MP, and Wilson WR (2012) Homologous recombination repair-dependent cytotoxicity of the benzotriazine di-N-oxide CEN-209: Comparison with other hypoxia-activated prodrugs. *Biochem Pharmacol* **83**:574–585.

Hunter FW, Wouters BG, and Wilson WR (2016) Hypoxia-activated prodrugs: Paths forward in the era of personalised medicine. *Br J Cancer* **114**:1071–1077.

Hunter FW, Young RJ, Shalev Z, Vellanki RN, Wang J, Gu Y, Joshi N, Sreebhavan S, Weinreb I, Goldstein DPDP, Moffat J, Ketela T, Brown KR, Koritzinsky M, Solomon B, Rischin D, Wilson WR, and Wouters BG (2015) Identification of P450 oxidoreductase as a major determinant of sensitivity to hypoxia-activated prodrugs. *Cancer Res* **75**:4211–4223.

Jamieson SMF, Tsai P, Kondratyev MK, Budhani P, Liu A, Senzer NN, Chiorean EG, Jalal SI,

Nemunaitis JJ, Kee D, Shome A, Wong WW, Li D, Poonawala-Lohani N, Kakadia PM, Knowlton NS, Lynch CRH, Hong CR, Lee TW, Grénman RA, Caporiccio L, McKee TD, Zaidi M, Butt S, Macann AMJ, McIvor NP, Chaplin JM, Hicks KO, Bohlander SK, Wouters BG, Hart CP, Print CG, Wilson WR, Curran MA, and Hunter FW (2018) Evofosfamide for the treatment of human papillomavirus-negative head and neck squamous cell carcinoma. *JCI insight* **3**:1–19.

Jayaprakash P, Ai M, Liu A, Budhani P, Bartkowiak T, Sheng J, Ager C, Nicholas C, Jaiswal A, Sun Y, Shah K, Balasubramanyam S, Li N, Wang G, Ning J, Zal A, Zal T, and Curran M (2018) Targeted hypoxia reduction restores T cell infiltration and sensitizes prostate cancer to immunotherapy. *J Clin Invest* **In press**.

Kim JW, Tchernyshyov I, Semenza GL, and Dang C V. (2006) HIF-1-mediated expression of pyruvate dehydrogenase kinase: A metabolic switch required for cellular adaptation to hypoxia. *Cell Metab* **3**:177–185.

King M, and Attardi G (1989) Human cells lacking mtDNA: repopulation with exogenous mitochondria by complementation. *Science (80-)* **246**:500–503.

Köchli H, Wermuth B, and von Wartburg J (1980) Characterization of a mitochondrial NADH-dependent nitro reductase from rat brain. *Biochim Biophys Acta* **616**:133–142.

Liu Q, Sun JD, Wang J, Ahluwalia D, Baker AF, Cranmer LD, Ferraro D, Wang Y, Duan JX, Ammons WS, Curd JG, Matteucci MD, and Hart CP (2012) TH-302, a hypoxia-activated prodrug with broad in vivo preclinical combination therapy efficacy: Optimization of dosing regimens and schedules. *Cancer Chemother Pharmacol* **69**:1487–1498.

Lohse I, Rasowski J, Cao P, Pintilie M, Do T, Taso MS, Hill RP, and Hedley DW (2016) Targeting hypoxic microenvironment of pancreatic xenografts with the hypoxia-activated prodrug TH-302. *Oncotarget* **7**:33571–33580.

Meissner B, Bartram T, Eckert C, Koehler R, Trka J, Hermanova I, Breithaupt P, Zimmermann M, Cario G, Schrauder A, Möricke A, Cazzaniga G, Kronnie G, Kirschner-Schwabe R, von Stackelberg A, Harbott J, Panzer-Gruemayer R, Bourquin J-P, Franke A, Ellinghaus E, Schreiber S, Bartram CR, Schrappe M, and Stanulla M (2010) C20orf94 deletion is strongly associated with TEL/AML1 rearrangement and links illegitimate V(D)J recombination with gender bias in

childhood acute lymphoblastic leukemia. *Blood* **116**:1718 LP-1718.

Meng F, Evans JW, Bhupathi D, Banica M, Lan L, Lorente G, Duan J-X, Cai X, Mowday AM, Guise CP, Maroz A, Anderson RF, Patterson A V., Stachelek GC, Glazer PM, Matteucci MD, and Hart CP (2012) Molecular and cellular pharmacology of the hypoxia-activated prodrug TH-302. *Mol Cancer Ther* **11**:740–751.

Naviaux RK (2008) Mitochondrial control of epigenetics. *Cancer Biol Ther* **7**:1191–1193.

Nogales V, Reinhold WC, Varma S, Martinez-Cardus A, Moutinho C, Moran S, Heyn H, Sebio A, Barnadas A, Pommier Y, and Esteller M (2015) Epigenetic inactivation of the putative DNA/RNA helicase SLFN11 in human cancer confers resistance to platinum drugs. *Oncotarget* **7**:3084–3097.

Nytko KJ, Grgic I, Bender S, Ott J, Riesterer O, and Pruschy M (2017) The hypoxia-activated prodrug evofosfamide in combination with multiple regimens of radiotherapy. **8**:23702–23712.

Papadopoulou M, Ji M, Rao M, and Bloomer W (2003) Reductive metabolism of the nitroimidazole-based hypoxia-selective cytotoxin NLCQ-1 (NSC 709257). *Oncol Res* **14**:21–29.

Papandreou I, Cairns RA, Fontana L, Lim AL, and Denko NC (2006) HIF-1 mediates adaptation to hypoxia by actively downregulating mitochondrial oxygen consumption. *Cell Metab* **3**:187–197.

Patterson A V., Saunders MP, Chinje EC, Talbot DC, Harris AL, and Stratford IJ (1997) Overexpression of human NADPH:cytochrome c (P450) reductase confers enhanced sensitivity to both tirapazamine (SR 4233) and RSU 1069. *Br J Cancer* **76**:1338–1347.

Peeters SGJA, Zegers CML, Biemans R, Lieuwes NG, Van Stiphout RGPM, Yaromina A, Sun JD, Hart CP, Windhorst AD, Van Elmpt W, Dubois LJ, and Lambin P (2015) TH-302 in combination with radiotherapy enhances the therapeutic outcome and is associated with pretreatment [18F]HX4 hypoxia PET imaging. *Clin Cancer Res* **21**:2984–2992.

Pham T, Loiselle D, Power A, and Hickey AJR (2014) Mitochondrial inefficiencies and anoxic ATP hydrolysis capacities in diabetic rat heart. *AJP Cell Physiol* **307**:C499–C507.

Sanjana NE, Shalem O, and Zhang F (2014) Improved vectors and genome-wide libraries for CRISPR screening. *Nat Methods* **11**:783–784.

Smiraglia DJ, Kulawiec M, Bistulfi GL, Gupta SG, and Keshav SK (2008) A novel role for

mitochondria in regulating epigenetic modification in the nucleus. *Cancer Biol Ther* **7**:1182–1190.

Smurnyy Y, Cai M, Wu H, McWhinnie E, Tallarico JA, Yang Y, and Feng Y (2014) DNA sequencing and CRISPR-Cas9 gene editing for target validation in mammalian cells. *Nat Chem Biol* **10**:623–625.

Su J, Gu Y, Pruijn FB, Smaill JB, Patterson A V., Guise CP, and Wilson WR (2013) Zinc finger nuclease knock-out of NADPH:cytochrome P450 oxidoreductase (POR) in human tumor cell lines demonstrates that hypoxia-activated prodrugs differ in POR dependence. *J Biol Chem* **288**:37138–37153.

Su J, Guise CP, and Wilson WR (2013) FSL-61 is a 6-nitroquinolone fluorogenic probe for one-electron reductases in hypoxic cells. *Biochem J* **452**:79–86.

Sun JD, Ahluwalia D, Liu Q, Li W, Wang Y, Meng F, Bhupathi D, Matteucci MD, and Hart CP (2015) Combination treatment with hypoxia-activated prodrug evofosfamide (TH-302) and mTOR inhibitors results in enhanced antitumor efficacy in preclinical renal cell carcinoma models. *Am J Cancer Res* **5**:2139–2155.

Sun JD, Liu Q, Wang J, Ahluwalia D, Ferraro D, Wang Y, Duan JX, Ammons WS, Curd JG, Matteucci MD, and Hart CP (2012) Selective tumor hypoxia targeting by hypoxia-activated prodrug TH-302 inhibits tumor growth in preclinical models of cancer. *Clin Cancer Res* **18**:758–770.

Svendsen JM, Smogorzewska A, Sowa ME, O'Connell BC, Gygi SP, Elledge SJ, and Harper JW (2009) Mammalian BTBD12/SLX4 assembles a Holliday junction resolvase and is required for DNA repair. *Cell* **138**:63–77.

Takakusagi Y, Kishimoto S, Sarwat N, Matsumoto S, Saito K, Hart C, Mitchell JB, and Cherukuri MK (2018) Radiotherapy synergizes with the hypoxia-activated prodrug evofosfamide. In vitro and in vivo studies. *Antioxid Redox Signal* **28**:131–140.

Takakusagi Y, Matsumoto S, Saito K, Matsuo M, Kishimoto S, Wojtkowiak JW, DeGraff W, Kesarwala AH, Choudhuri R, Devasahayam N, Subramanian S, Munasinghe JP, Gillies RJ, Mitchell JB, Hart CP, and Krishna MC (2014) Pyruvate induces transient tumor hypoxia by

enhancing mitochondrial oxygen consumption and potentiates the anti-tumor effect of a hypoxia-activated prodrug TH-302. *PLoS One* **9**:1–10.

Tap WD, Papai Z, Van Tine BA, Attia S, Ganjoo KN, Jones RL, Schuetze S, Reed D, Chawla SP, Riedel RF, Krarup-Hansen A, Toulmonde M, Ray-Coquard I, Hohenberger P, Grignani G, Cranmer LD, Okuno S, Agulnik M, Read W, Ryan CW, Alcindor T, del Muro XFG, Budd GT, Tawbi H, Pearce T, Kroll S, Reinke DK, and Schöffski P (2017) Doxorubicin plus evofosfamide versus doxorubicin alone in locally advanced, unresectable or metastatic soft-tissue sarcoma (TH CR-406/SARC021): an international, multicentre, open-label, randomised phase 3 trial. *Lancet Oncol* **18**:1089–1103.

Tian Y, Zhang J, Yan S, Qiu L, and Li Z (2012) FATS expression is associated with cisplatin sensitivity in non small cell lung cancer. *Lung Cancer* **76**:416–422.

Trédan O, Galmarini CM, Patel K, and Tannock IF (2007) Drug resistance and the solid tumor microenvironment. *J Natl Cancer Inst* **99**:1441–1454.

Vanderkooi JM, Glatz P, Casadei J, and Woodrow III G V. (1980) Cytochrome c interaction with yeast cytochrome b2: Heme distances determined by energy transfer in fluorescence resonance. *Eur J Biochem* **110**:189–196.

Vyas S, Zaganjor E, and Haigis MC (2016) Mitochondria and cancer. *Cell* **166**:555–566.

Wang J, Foehrenbacher A, Su J, Patel R, Hay MP, Hicks KO, and Wilson WR (2012) The 2-nitroimidazole EF5 is a biomarker for oxidoreductases that activate the bioreductive prodrug CEN-209 under hypoxia. *Clin Cancer Res* **18**:1684–1695.

Wang J, Guise CP, Dachs GU, Phung Y, Hsu AHL, Lambie NK, Patterson A V., and Wilson WR (2015) Identification of one-electron reductases that activate both the hypoxia prodrug SN30000 and diagnostic probe EF5. *Biochem Pharmacol* **91**:436–446.

Weiss GJ, Infante JR, Chiorean EG, Borad MJ, Bendell JC, Molina JR, Tibes R, Ramanathan RK, Lewandowski K, Jones SF, Lacouture ME, Langmuir VK, Lee H, Kroll S, and Burris HA (2011) Phase 1 study of the safety, tolerability, and pharmacokinetics of TH-302, a hypoxia-activated prodrug, in patients with advanced solid malignancies. *Clin Cancer Res* **17**:2997–3004.

Wilson WR, and Hay MP (2011) Targeting hypoxia in cancer therapy. *Nat Rev Cancer* **11**:393–410.

Zhang L, Marrano P, Wu B, Kumar S, Thorner P, and Baruchel S (2016) Combined antitumor therapy with metronomic topotecan and hypoxia-activated prodrug, evofosfamide, in neuroblastoma and rhabdomyosarcoma preclinical models. *Clin Cancer Res* **22**:2697–2708.

Zoppoli G, Regairaz M, Leo E, Reinhold WC, Varma S, Ballestrero A, Doroshow JH, and Pommier Y (2012) Putative DNA/RNA helicase Schlafen-11 (SLFN11) sensitizes cancer cells to DNA-damaging agents. *Proc Natl Acad Sci* **109**:15030–15035.

Molecular Pharmacology Fast Forward. Published on April 12, 2019 as DOI: 10.1124/mol.118.115196
This article has not been copyedited and formatted. The final version may differ from this version.

Footnotes

Financial Support. This research was supported by the Cancer Society of New Zealand [project grant 15.16]; the Cancer Research Trust New Zealand [John Gavin Postdoctoral Fellowship GOT-1438-JGPDF]; the Royal Society Te Apārangi [Rutherford Foundation Postdoctoral Fellowship RFT-UOA1601-PD and Marsden grant 14-UOA-121]; the Health Research Council of New Zealand [Programme grant 14/538]; and the Family of Marijana Kumerich and Leukaemia & Blood Cancer New Zealand [endowed chair].

Meeting Abstract. Hunter et al., 2017. Abstract 169: Preclinical efficacy and sensitivity determinants of evofosfamide in molecularly defined models of head and neck squamous cell carcinoma. *Cancer Research* 77(13 Supplement):169-169. Proceedings: AACR Annual Meeting 2017; April 1-5, 2017; Washington, DC.

Reprint Requests. Dr Francis W. Hunter, Auckland Cancer Society Research Centre, University of Auckland, Private Bag 92019, Auckland, New Zealand. Email: f.hunter@auckland.ac.nz.

Molecular Pharmacology Fast Forward. Published on April 12, 2019 as DOI: 10.1124/mol.118.115196
This article has not been copyedited and formatted. The final version may differ from this version.

Figure Legends

Fig. 1. Antiproliferative activity of evofosfamide in cancer cell lines. (A) Schema of the mechanism of reductive activation and hypoxia selectivity of evofosfamide. The 2-nitroimidazole moiety of evofosfamide undergoes enzymatic one-electron reduction to yield a short-lived radical anion. In the absence of oxygen, the latter fragments (frag.) to release the DNA-crosslinking effector bromo-*iso*-phosphoramide (Br-IPM), which is spontaneously converted to Cl-IPM by halide exchange. In the presence of oxygen, the radical is back-oxidised to the parent prodrug in kinetic competition with fragmentation. (B) Antiproliferative activity and hypoxic selectivity of evofosfamide in a diverse panel of 32 human cancer cell lines. Cells in 24-well plates were exposed to a dilution series of evofosfamide for 2 h under anoxia (N_2) or 20% O_2 with 5% CO_2 (Air) then cultured aerobically for 7 d in drug-free medium prior to assessment of culture density by alamarBlue assay. The drug concentrations for half-maximal inhibition of cell growth relative to vehicle-treated control wells on the same plate (IC_{50}) were computed by four-parameter functions to the data. Data are presented as the mean + SEM of three independent experiments. (C) Correlation between the antiproliferative potency of evofosfamide as assessed in cancer cell lines using 3-d or 7-d regrowth assays. The former dataset has been published previously (Meng *et al.*, 2012). Data are the mean ± SEM of three independent experiments.

Fig. 2. The expression of genes implicated in mitochondrial biology correlates with evofosfamide sensitivity in cancer cell lines. (A) Pairwise correlation structure of transcriptional profiles in 30 cancer cell lines also tested for *in vitro* sensitivity to evofosfamide. RNAseq data were sourced from the Cancer Cell Line Encyclopedia and RSEM counts were $\log_2$ transformed and quantile normalised. Pairwise Spearman correlation coefficients for the resulting count distributions are plotted in the heatmap. (B) The relationship between gene expression features and evofosfamide sensitivity in cancer cell lines. The heatmap illustrates the expression of the 173 genes inversely correlated with evofosfamide sensitivity under anoxia with a Pearson coefficient ≤ -0.4. The cell lines in the cluster are ranked in ascending order by the first principal component of expression values for these 173 genes, with the relationship between

Molecular Pharmacology Fast Forward. Published on April 12, 2019 as DOI: 10.1124/mol.118.115196
This article has not been copyedited and formatted. The final version may differ from this version.

this variable and evofosfamide IC_{50} under anoxia indicated. (C) An interacting protein network among genes correlated with evofosfamide potency as per (B). The network was generated using the STRING database (string-db.org) and gene functions of clusters within the network annotated using GeneSetDB (genesetdb.auckland.ac.nz). The number of edges (protein-protein interactions) in the network (n=166) was significantly greater than expected by random sampling (E(n)=82; $p<10^{-15}$).

Fig. 3. A whole-genome CRISPR knockout screen for modifiers of evofosfamide sensitivity identifies mitochondrial respiration and DNA damage response. (A) Abstracted workflow for functional screens using lentiviral whole-genome sgRNA and focused shRNA libraries (results of the latter are reported in Fig. 4) to identify genetic modifiers of sensitivity to evofosfamide. (B) Growth kinetics of KBM-7 cultures transduced with the GeCKOv2 sgRNA library and treated with evofosfamide or control vehicle. Data points are the mean ± SEM of the cumulative fold increase in population size relative to starting cultures for three biological replicates of each condition. Red arrows denote the times of challenge with 0.013 μM evofosfamide. The growth of evofosfamide-treated cultures was inhibited by a factor of 10^4 relative to vehicle control. (C) Assessment of evofosfamide sensitivity by IC_{50} assay in drug-challenged and naïve KBM-7 knockout libraries at the endpoint of the CRISPR screen. Data points are the mean ± SEM of cell viability determinations at each evofosfamide concentration for three replicate cultures from the CRISPR screen. Dose-modifying factor (DMF) was defined as the ratio of IC_{50} values in evofosfamide-challenged relative to naïve cultures. (D) Deconvolution of the CRISPR screen using the MAGeCK statistical algorithm. The statistical significance of positive or negative selection of sgRNA targets is plotted as a function of the median $\log_2$ fold change in the representation of sgRNA against each target. Select high ranking findings are highlighted. (E) Comparison of hits called in positive selection in the CRISPR screen using the MAGeCK and PinAPL-Py algorithms. Targets called as positively selected beyond a statistical threshold of P<0.005 by either method are coloured red, with select high ranking hits further highlighted. (F) An interacting protein network among gene knockouts positively selected by evofosfamide treatment in the CRISPR screen (targets in red in E). The network was generated using the STRING database (string-db.org) and gene functions of clusters within the network annotated using GeneSetDB (genesetdb.auckland.ac.nz). The number of edges (protein-protein

Molecular Pharmacology Fast Forward. Published on April 12, 2019 as DOI: 10.1124/mol.118.115196
This article has not been copyedited and formatted. The final version may differ from this version.

interactions) in the network (n=37) was significantly greater than expected by random sampling (E(n)=18; $p<10^{-4}$).

Fig. 4. An oxidoreductase-focused shRNA screen identifies mitochondria-related genes potentially involved in determining evofosfamide sensitivity. (A) Plating efficiency of UT-SCC-74B cells immediately prior to the addition of evofosfamide ("baseline"), immediately after the completion of evofosfamide exposure ("post-EVO") and after recovery of the cultures. The surviving fraction of 10^{-3} was determined as the ratio of plating efficiencies after and before evofosfamide exposure. Data points are from 2-3 determinations and the mean ± SEM is shown. (B) Deconvolution of the shRNA screen using the MAGeCK and RIGER algorithms, the latter using weighted-sum aggregation to generate gene-level significance scores. The statistical significance of positive selection hits is plotted for the two deconvolution methods, with select high ranking candidates highlighted. (C) An interacting protein network among gene knockouts positively selected by evofosfamide in the shRNA screen (P<0.05 by MAGeCK, RIGER or PinAPL-Py). The network was generated using the STRING database (string-db.org) and gene functions of clusters within the network annotated using GeneSetDB (genesetdb.auckland.ac.nz). The number of edges (protein-protein interactions) in the network (n=82) was significantly greater than expected by random sampling (E(n)=11; $p<10^{-16}$).

Fig. 5. Rho zero cells deficient in mitochondrial DNA show enhanced bioreductive prodrug activation and sensitivity. (A) Confirmation of the absence of mitochondrial DNA in ρ^0 cells derived from the 143B osteosarcoma cell line. Endpoint PCR for amplification of mitochondrial-encoded *MT-TL1* (tRNA leucine 1) relative to nuclear-encoded *GAPDH* was used to demonstrate the absence of mitochondrial genomes in ρ^0 cells. (B) Mitochondrial respiration rates in 143B and ρ^0 cells in LEAK state (respiration attributed to proton leak in non-phosphorylating mitochondria), OXPHOS (maximum rate of oxidative phosphorylation), CII (maximum electron entry at complex II from succinate forced by complex I inhibition with rotenone) and CIV (maximum activity of complex IV with TMPD and ascorbate). Data are mean ± SEM from five independent experiments and statistical significance of differences in respiration rates for each state was assessed using way-way ANOVA with Benjamini−Hochberg

Molecular Pharmacology Fast Forward. Published on April 12, 2019 as DOI: 10.1124/mol.118.115196
This article has not been copyedited and formatted. The final version may differ from this version.

adjustment for multiple comparisons. (C) Assessment of reductive activation of evofosfamide in 143B and ρ^0 cells by LC−MS/MS measurement of total Br-IPM, Cl-IPM and the 2-nitroimidazole fragmentation product ('Tr-H') concentrations at the endpoint of one-hour exposures to 30 μM evofosfamide under anoxia (24-well format, 10^6 cells/0.5 mL in each well). Data are the mean + SEM of metabolite concentrations for the sum of intracellular and extracellular metabolites (measured separately then summed), per culture, from five independent experiments. Statistical significance was assessed using Student's t-test operating on the sum of Br-IPM and Cl-IPM concentrations. (D) Enhanced reductive activation of the fluorogenic 6-nitroquinolone FSL-61 and the 2-nitroimidazole probe EF5 by ρ^0 cells under anoxia. The flow cytometry histograms illustrate fluorescence area event distributions for 143B, ρ^0 and unstained ρ^0 cells, where fluorescence originated from the reduced product of FSL-61 (Su, Guise, *et al.*, 2013) or an Alexa488-conjugated secondary antibody against cell-bound EF5 metabolites. The figures are representative of three independent experiments performed. The nitro moieties that are substrates for bioreduction are coloured red in each structure. (E) Enhanced sensitivity to bioreductive prodrugs in ρ^0 cells under anoxia. IC_{50} values for parental 143B cells and ρ^0 cells treated under normoxia ("air") and anoxia ("N_2") are shown for evofosfamide, the nitroaromatic mustard prodrug PR-104A and the benzotriazine di-*N*-oxide prodrug SN30000. Data points are from three independent experiments and the mean ± SEM is shown.

Fig. 6. Widespread changes in gene expression in 143B ρ^0 cells. (A) Heatmap of 6,740 genes determined to be differentially expressed in ρ^0 cells relative to parental 143B cells using the *limma* method ($P<0.05$ after adjustment for multiple comparisons using the Benjamini–Hochberg method). Functions enriched (Benjamini–Hochberg adjusted *P*-values < 0.05) among differentially expressed gene clusters were annotated using GeneSetDB (genesetdb.auckland.ac.nz) and the PANTHER database (pantherdb.org). (B) Reduced and increased (C) expression of genes involved DNA damage response and repair genes in ρ^0 cells. (D) Increased expression of flavoproteins in ρ^0 cells. For A-D, triplicate ρ^0 and 143B samples, were hierarchically clustered without supervision using the ward.D method with Euclidean distance. The heatmap scales denote row Z-scores for the triplicate samples arrayed in columns, where rows correspond to individual genes, for quantile-normalised, $\log_2$-transformed RSEM counts.

Molecular Pharmacology Fast Forward. Published on April 12, 2019 as DOI: 10.1124/mol.118.115196
This article has not been copyedited and formatted. The final version may differ from this version.

Fig. 7. Evofosfamide oxidises mitochondrial cytochromes and inhibits respiration in permeabilised UT-SCC-74B cells. (A) Absorption spectra of the mitochondrial cytochromes by spectrophotometry in permeabilised UT-SCC-74B cells exposed to graded evofosfamide with ambient O_2 relative to untreated controls. (B) Concentration-dependent oxidation of cytochromes *a*, *b* and *c* in permeabilised UT-SCC-74B cells exposed to evofosfamide. The relative contribution of each cytochrome to the absorbance in (A) was determined using extinction coefficients and the resulting oxidation state was normalised by the maximum reduction state of each cytochrome (induced using KCN). Curves represent independent experiments. (C) Assessment of ROS production by Amplex UltraRed assay in permeabilised UT-SCC-74B cells exposed to increasing concentrations of evofosfamide or corresponding volumes of DMSO vehicle. Data points are the mean ± SEM of determinations from at least four independent experiments. (D) Concentration-dependent inhibition of mitochondrial respiration in permeabilised UT-SCC-74B cells. Data points are the mean ± SEM of determinations from five independent experiments. (E) Inhibition of respiration by evofosfamide (200 μM) in permeabilised UT-SCC-74B cells in the LEAK (attributed to proton leak in non-phosphorylating mitochondria), OXPHOS (fully-active electron transport chain), CII (electron entry at complex II from succinate forced by inhibiting complex I with rotenone) and CIV (maximum capacity of CIV to reduce O_2) states. Data are mean + SEM of determinations from five independent experiments and statistical significance of differences in respiration rates for each state was assessed using two-way ANOVA with Benjamini−Hochberg adjustment for multiple comparisons. (F) Potential mechanism for reduction of evofosfamide via the interception of electrons from the mitochondrial transport chain.

Molecular Pharmacology Fast Forward. Published on April 12, 2019 as DOI: 10.1124/mol.118.115196
This article has not been copyedited and formatted. The final version may differ from this version.

Tables

TABLE 1

GO terms overrepresented among expressed genes that correlated with evofosfamide IC_{50} in cancer cell lines treated under anoxia

Genes with expression levels that were inversely correlated with evofosfamide IC_{50} values under anoxia (Pearson coefficient ≤ –0.4, which defined 173 genes) were assessed for overrepresentation of GO annotations using Fisher's exact tests. The resulting *P*-values were adjusted for multiple comparisons (i.e. all possible GO terms) using the Benjamini–Hochberg method. The fold enrichment of each significant (adjusted P-value < 0.05) GO annotation (i.e. the ratio of the actual to the expected number of genes on the list with the annotation given random sampling) is denoted.

GO term	Fold enrichment	Adj. *P*-value
GO0005743: Mitochondrial inner membrane	5.29	$<10^{-7}$
GO0005759: Mitochondrial matrix	5.10	10^{-4}
GO0005840: Ribosome	6.69	10^{-3}
GO0044822: Poly(A) RNA binding	2.34	0.002
GO0005739: Mitochondrion	2.45	0.009
GO0046872: Metal ion binding	1.93	0.009
GO0070125: Mitochondrial translational elongation	2.39	0.02
GO0070126: Mitochondrial translational termination	11.58	0.03

Molecular Pharmacology Fast Forward. Published on April 12, 2019 as DOI: 10.1124/mol.118.115196
This article has not been copyedited and formatted. The final version may differ from this version.

TABLE 2

GO terms overrepresented among sgRNA targets positively selected following evofosfamide selection of KBM-7 cells in a whole-genome CRISPR knockout screen

Gene targets called to be positively selected at a statistical significance threshold of $P \leq 0.005$ using the MAGeCK or PinAPL-Py screen deconvolution algorithms, or both, were included in the analysis. *P*-values for GO enrichment from Fisher's exact tests were adjusted for multiple comparisons using the Benjamini–Hochberg method.

GO term		Fold enrichment	Adj. *P*-value
GO0005747:	Mitochondrial respiratory chain complex I	17.71	0.004
GO0032981:	Mitochondrial respiratory chain complex I assembly	15.29	0.004
GO0008137:	NADH dehydrogenase (ubiquinone) activity	17.16	0.008
GO0006120:	Mitochondrial electron transport, NADH to ubiquinone	16.85	0.008

Molecular Pharmacology Fast Forward. Published on April 12, 2019 as DOI: 10.1124/mol.118.115196
This article has not been copyedited and formatted. The final version may differ from this version.

TABLE 3

GO terms overrepresented among shRNA targets positively selected following evofosfamide selection of UT-SCC-74B cells in a reductase-focused RNAi screen

Gene targets called to be positively selected at a statistical significance threshold of P <0.05 using the MAGeCK, PinAPL-Py or RIGER screen deconvolution algorithms were included in the analysis. *P*-values for GO enrichment arising from Fisher's exact tests were adjusted using the Benjamini–Hochberg method.

GO term	Fold enrichment	Adj. *P*-value
GO0005740: Mitochondrial envelope	2.80	0.002
GO0044455: Mitochondrial membrane part	3.94	0.002
GO0070469: Respiratory chain	3.78	0.002
GO0031967: Organelle envelope	2.65	0.003
GO0031975: Envelope	2.65	0.003
GO0005746: Mitochondrial respiratory chain	3.90	0.004
GO0031966: Mitochondrial membrane	2.61	0.006
GO0006091: Generation of precursor metabolites and energy	3.08	0.01
GO0005743: Mitochondrial inner membrane	2.54	0.01
GO0019866: Organelle inner membrane	2.54	0.01
GO0044429: Mitochondrial part	2.18	0.01
GO0005747: Mitochondrial respiratory chain complex I	4.62	0.01
GO0045271: Respiratory chain complex I	4.62	0.01
GO0030964: NADH dehydrogenase complex	4.62	0.01
GO0022900: Electron transport chain	3.15	0.02

Molecular Pharmacology Fast Forward. Published on April 12, 2019 as DOI: 10.1124/mol.118.115196
This article has not been copyedited and formatted. The final version may differ from this version.

GO0051536:	Iron-sulfur cluster binding	5.69	0.02
GO0051540:	Metal cluster binding	5.69	0.02
GO0045333:	Cellular respiration	3.94	0.03
GO0005739:	Mitochondrion	1.73	0.03
GO0015980:	Energy derivation by oxidation of organic compounds	3.78	0.03
GO0050136:	NADH dehydrogenase (quinone) activity	5.25	0.03
GO0008137:	NADH dehydrogenase (ubiquinone) activity	5.25	0.03
GO0003954:	NADH dehydrogenase activity	5.25	0.03
GO0006119:	Oxidative phosphorylation	4.05	0.03
GO0031090:	Organelle membrane	1.85	0.04
GO0051539:	4 iron, 4 sulfur cluster binding	7.32	0.04

Molecular Pharmacology Fast Forward. Published on April 12, 2019 as DOI: 10.1124/mol.118.115196
This article has not been copyedited and formatted. The final version may differ from this version.

Figures

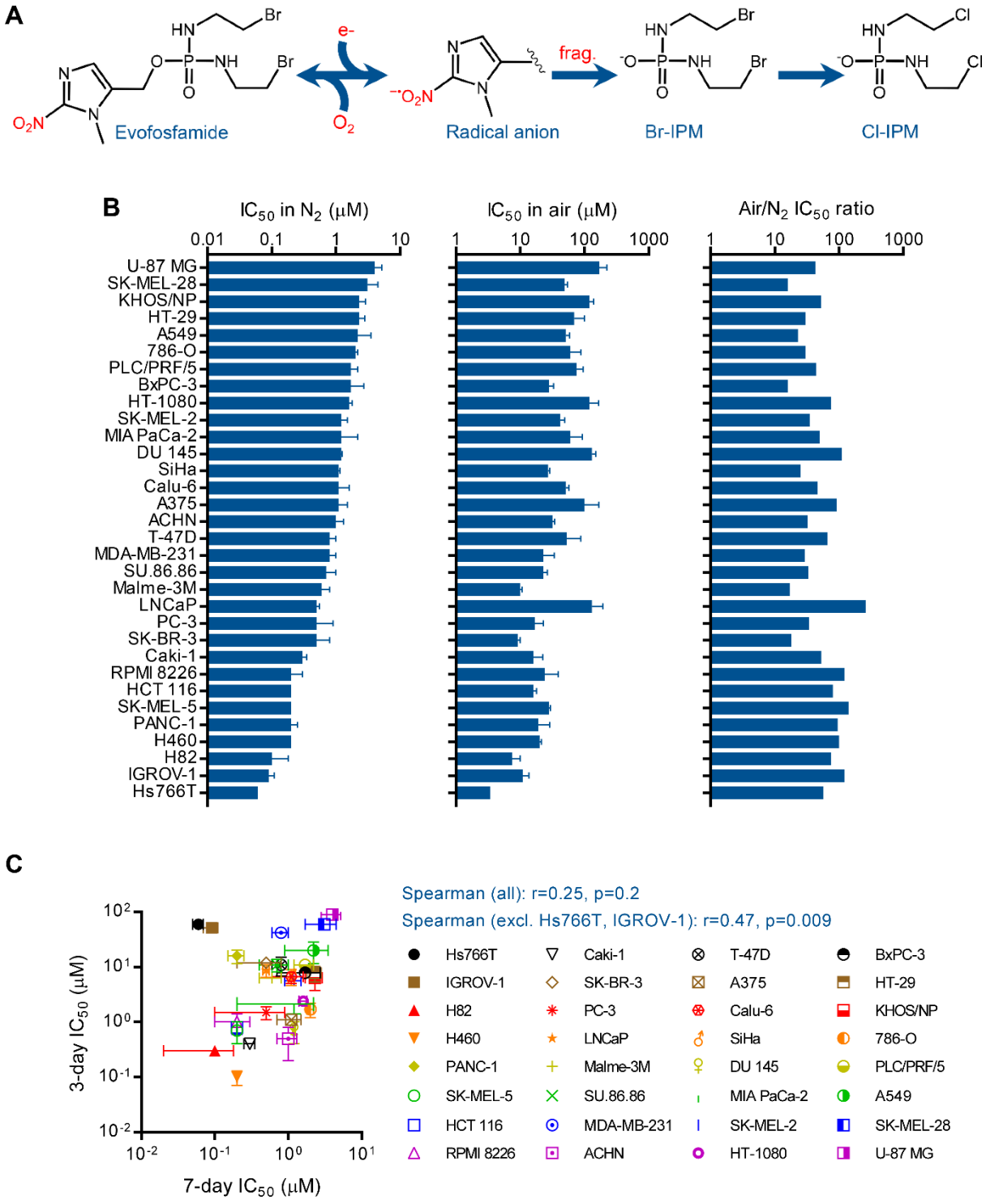

Figure 1

Molecular Pharmacology Fast Forward. Published on April 12, 2019 as DOI: 10.1124/mol.118.115196
This article has not been copyedited and formatted. The final version may differ from this version.

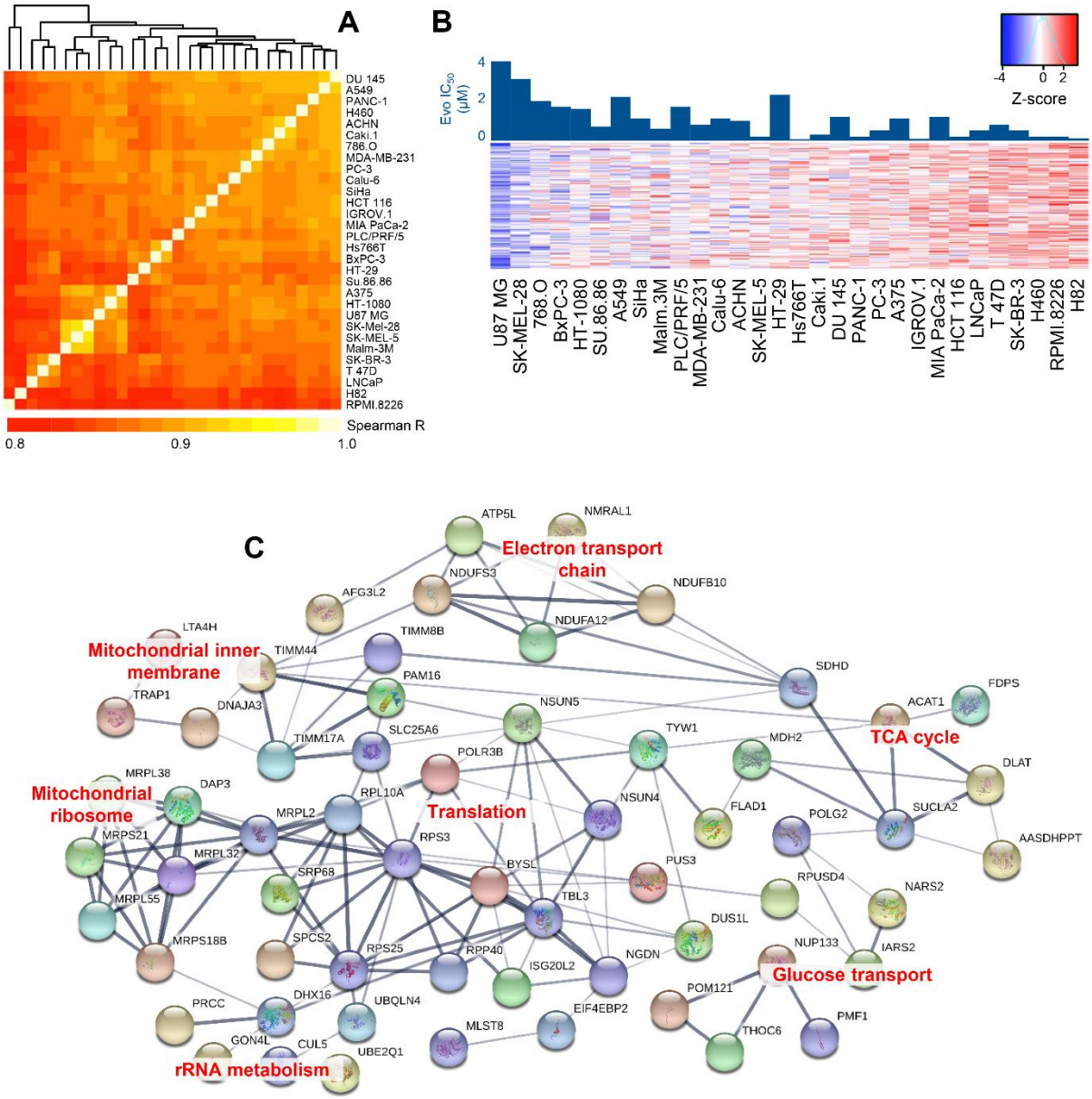

Figure 2

Molecular Pharmacology Fast Forward. Published on April 12, 2019 as DOI: 10.1124/mol.118.115196
This article has not been copyedited and formatted. The final version may differ from this version.

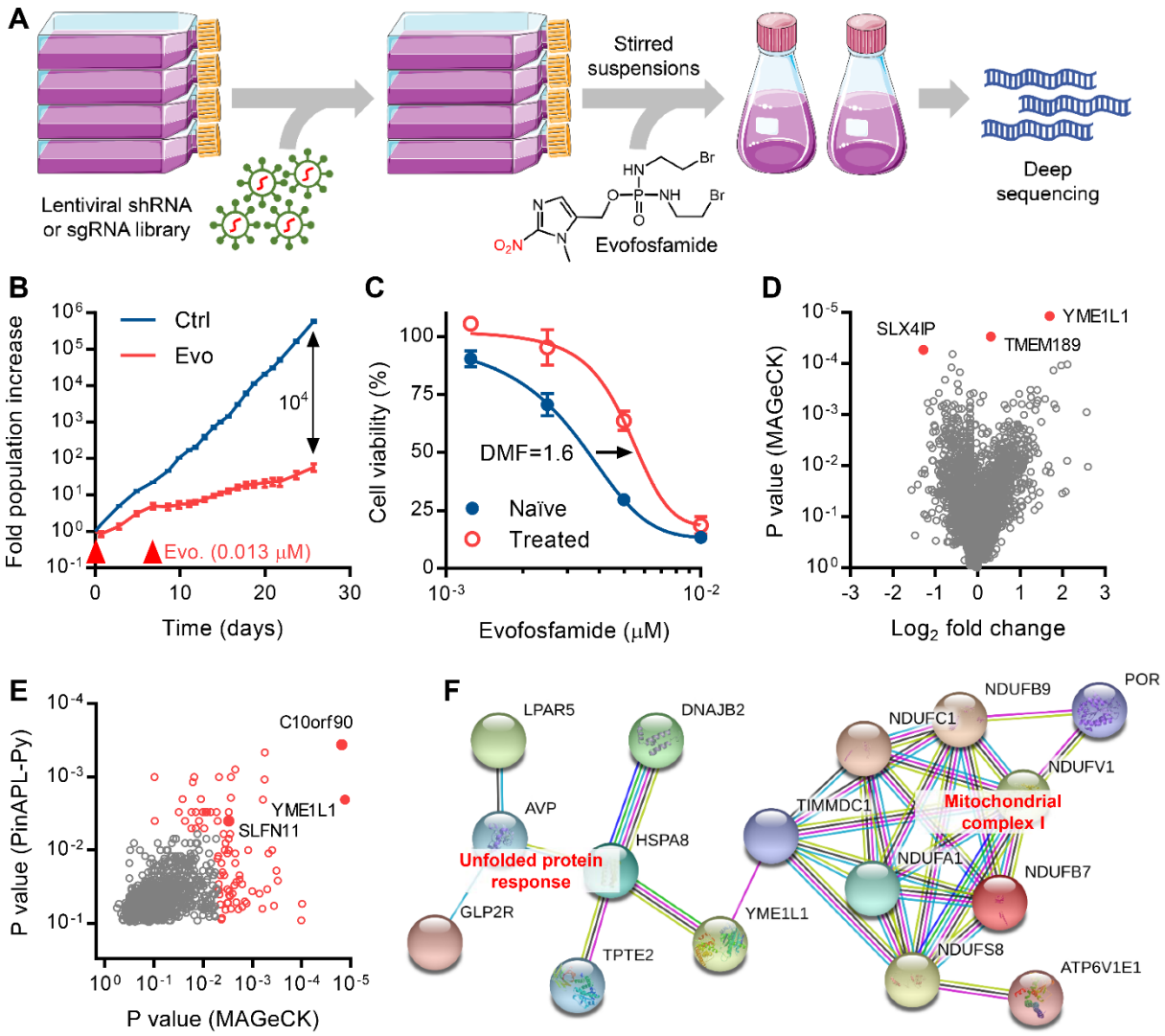

Figure 3

Molecular Pharmacology Fast Forward. Published on April 12, 2019 as DOI: 10.1124/mol.118.115196
This article has not been copyedited and formatted. The final version may differ from this version.

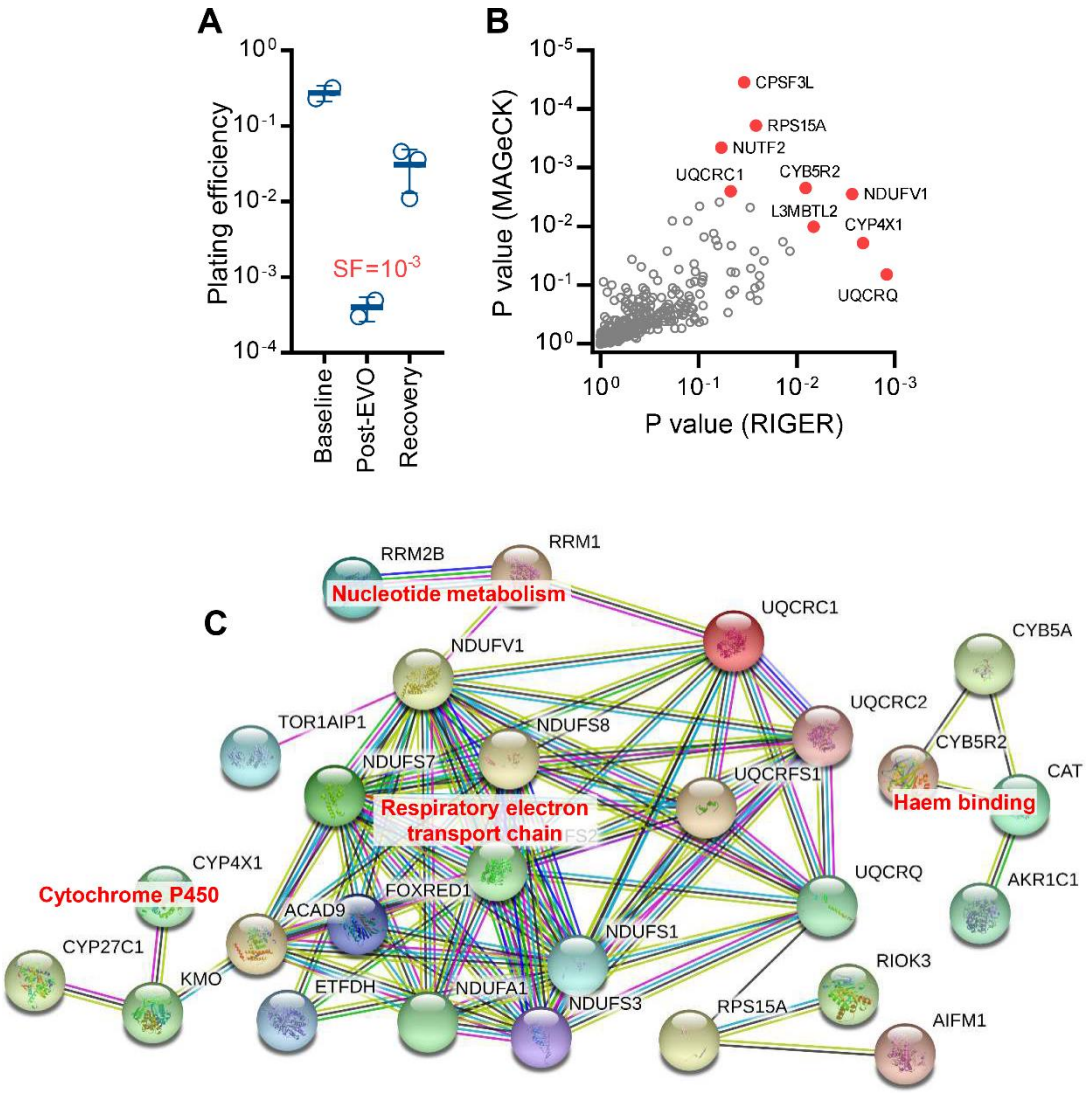

Figure 4

Molecular Pharmacology Fast Forward. Published on April 12, 2019 as DOI: 10.1124/mol.118.115196
This article has not been copyedited and formatted. The final version may differ from this version.

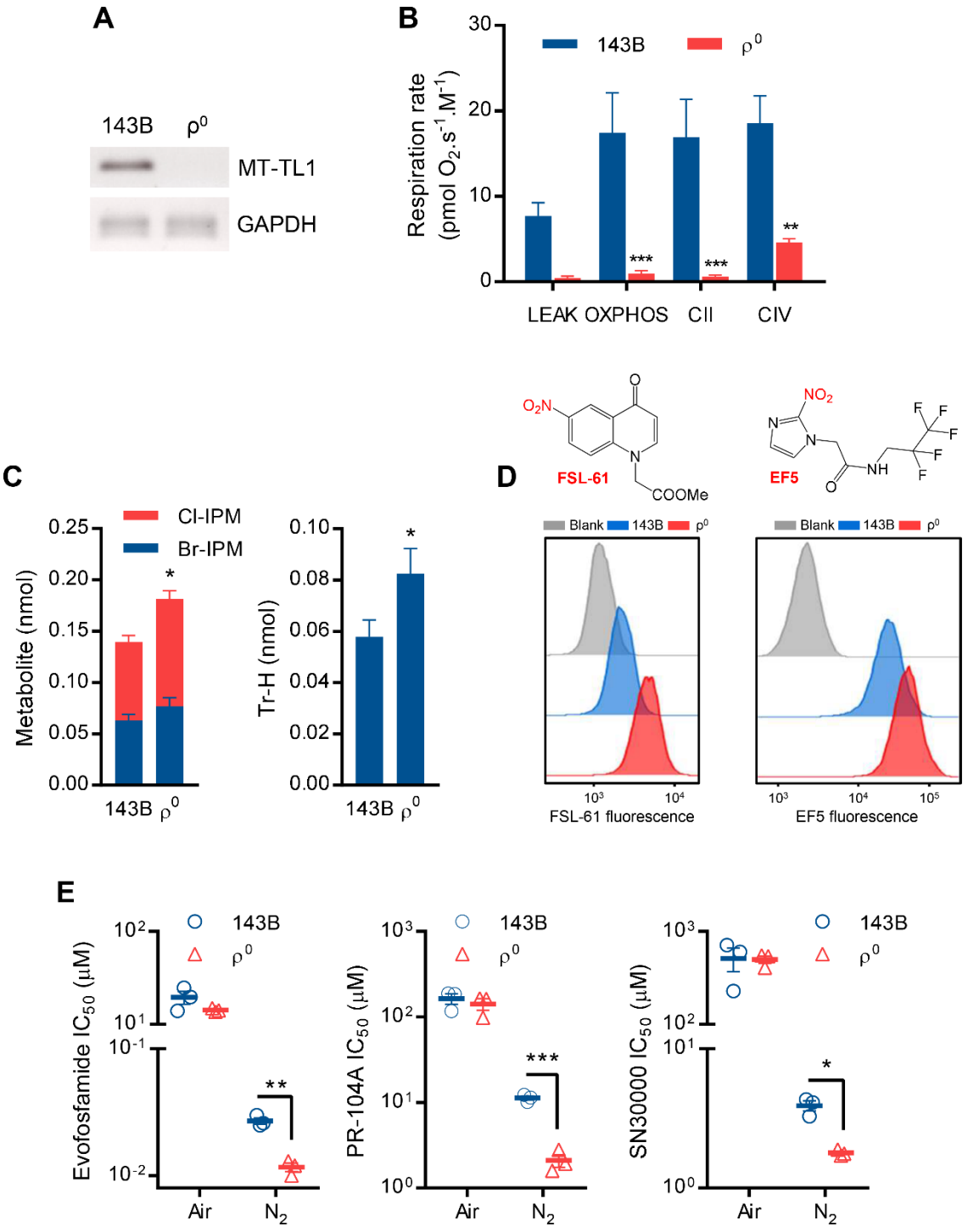

Figure 5

Molecular Pharmacology Fast Forward. Published on April 12, 2019 as DOI: 10.1124/mol.118.115196
This article has not been copyedited and formatted. The final version may differ from this version.

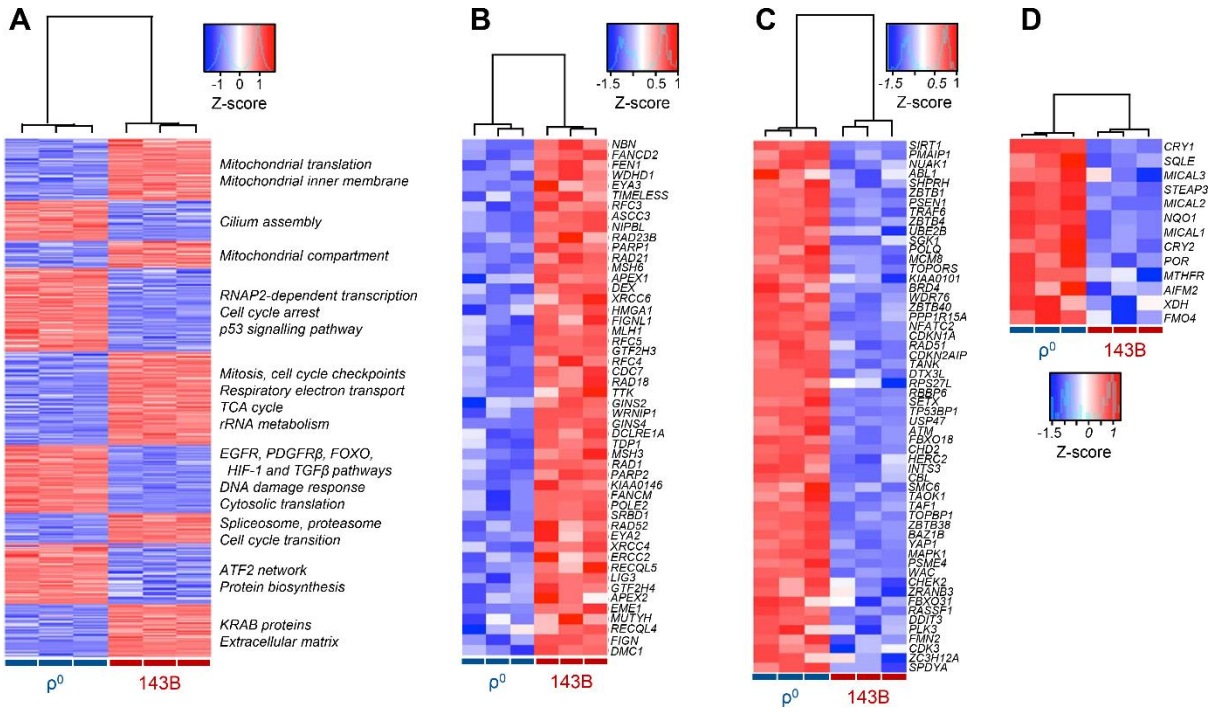

Figure 6

Molecular Pharmacology Fast Forward. Published on April 12, 2019 as DOI: 10.1124/mol.118.115196
This article has not been copyedited and formatted. The final version may differ from this version.

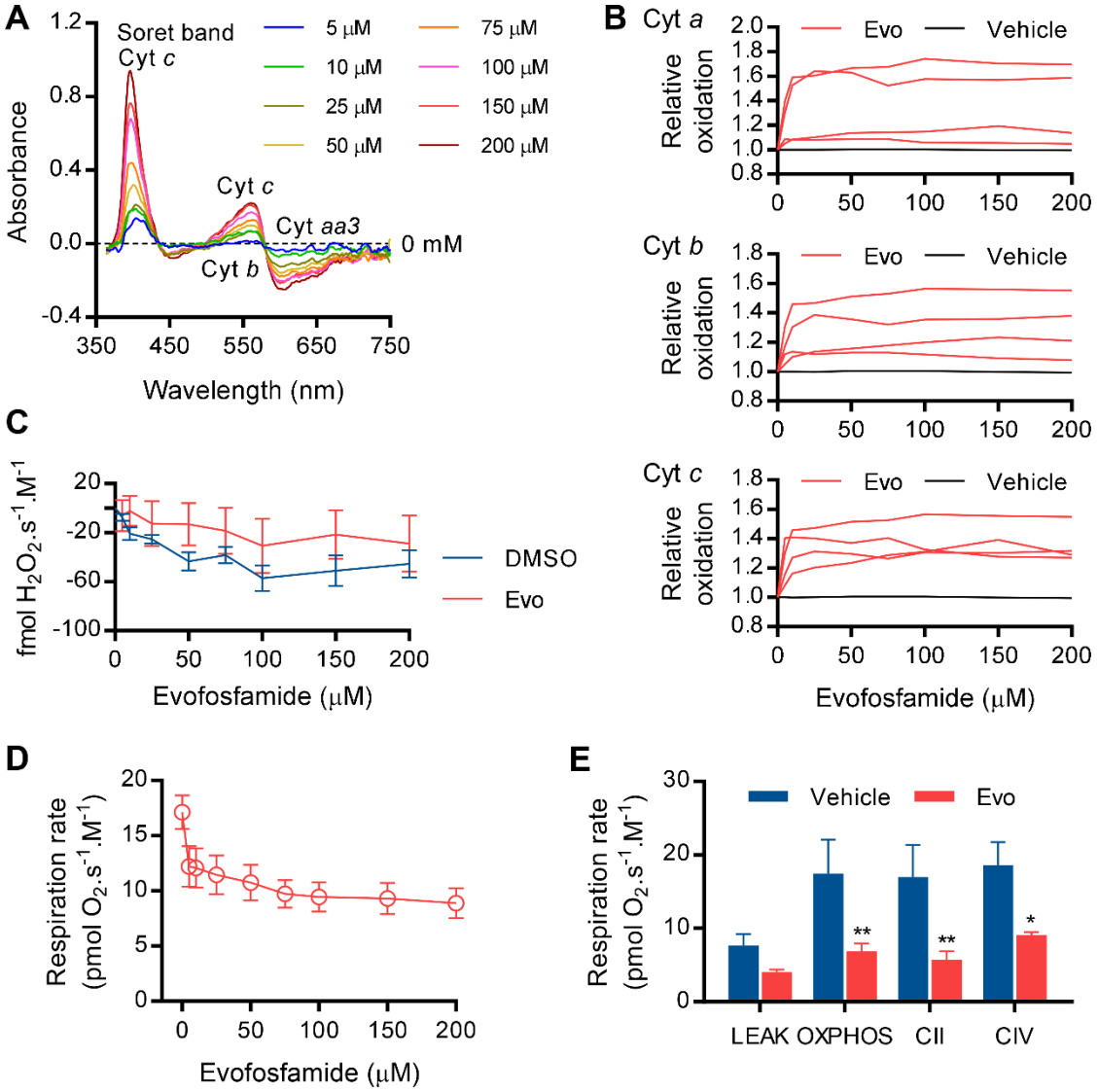

Figure 7